Journal of Magnetism and Magnetic Materials 551 (2022) 169185

Contents lists available at ScienceDirect

Journal of Magnetism and Magnetic Materials

journal homepage: www.elsevier.com/locate/jmmm

Quantitative characterisation and modelling of the effect of cut edge damage on the magnetic properties in NGO electrical steel

Fanfu Wu *, Lei Zhou, Juliette Soulard, Ben Silvester, Claire Davis

WMG, University of Warwick, Coventry CV4 7AL, UK

ARTICLE INFO

Keywords:
Non-oriented electrical steel
Strain of stamped edge
Magnetic properties
BH curve
Cut edge characterisation

ABSTRACT

The cut edges of electrical steel NGO laminations in electric motors experience mechanically induced plastic deformation and residual elastic stress, which deteriorate the magnetic performance of the material. This deterioration is accounted for empirically in electric machine modelling tools by introducing a 'build factor' on the iron losses. Currently, a wide range of cut edge deteriorated widths have been reported in the literature, depending on the method used for characterisation, the material and the cutting method. In this paper, cut edge plastic damage characterisation was carried out using EBSD kernel average misorientation (KAM) maps and nano-indentation to quantify the magnitude and width of the plastic damage at the cut edge for a stamped tooth of a segmented stator and a guillotined single sheet tester (SST) sample. The relationship between the EBSD KAM and nano-hardness values and plastic strain was found using tensile samples tested to varying applied strain levels. Therefore, the plastic strain gradient with respect to distance from the cut edge was determined. It was found that both EBSD and nano-indentation gave similar predictions of effective plastic strain values and damage width: up to 1.45–1.50 at stamped cut edge over 180 μm width and up to 1.35–1.4 at guillotine cut edge over 250 μm width. The relationships between the magnetic performance and elastic stress, plastic strain, and plastic strain with elastic stress were determined using single sheet tester (SST) measurements. In addition, SST 3D FEA models of the cut edge sample were built using COMSOL Multi-Physics software considering a single layer for plastic damage only and two layers for plastic damage + elastic stress and elastic stress. The modelling results for the guillotine cut edge SST samples were compared to measured data. It was found that to obtain accurate cut edge magnetic property deterioration for NGO electrical steel laminations both the plastic strain and residual elastic stress cut edge effects need to be included. In the cut edge model, a first layer width of 250 μm with magnetic properties for an effective plastic strain of 1.17 under residual compressive elastic stress of −133 MPa and a second layer width of 220 μm with magnetic properties for residual compressive elastic stress of −119 MPa give excellent results for hysteretic BH curves and specific iron loss evaluation.

1. Introduction

Predicting the performance of electrical machines is challenging with a significant trade-off between model accuracy and calculations cost. Often models incorporating complex phenomena are not viable due to time and cost. Therefore, discrepancies between calculated and measured motor losses are accounted for by build factors, multipliers to the calculated loss values [1,2] The 'build factors' are catch-all terms covering changes in calculation inaccuracy, material properties, damage due to manufacturing processes and geometrical defects. Often considered a fixed multiplier, the build factor value for iron loss can vary between 1.1 and 2.7, 10% or 270% extra loss [2–4]. During motor manufacturing, magnetic property deterioration from NGO electrical steel lamination cut edge damage is unavoidable and increases the iron loss [5–9] a detriment to motor performance [3,4,10–13]. Cut edge damage has been estimated to account for approximately 10–40% increase in iron loss, based on motor measurements [4]. The percentage contribution of cut-edge to the whole build factor is dependent on the motor topology, motor geometry, selected manufacturing processes and materials used.

At the lamination cut edge, there is a mechanically induced plastic deformation region with reported widths varying from several tens of micrometres to several millimetres depending on the grade of NGO electrical steels and experimental characterisation method. The

* Corresponding author.
E-mail address: fanfu.wu@warwick.ac.uk (F. Wu).

https://doi.org/10.1016/j.jmmm.2022.169185
Received 17 November 2021; Received in revised form 20 January 2022; Accepted 15 February 2022
Available online 17 February 2022

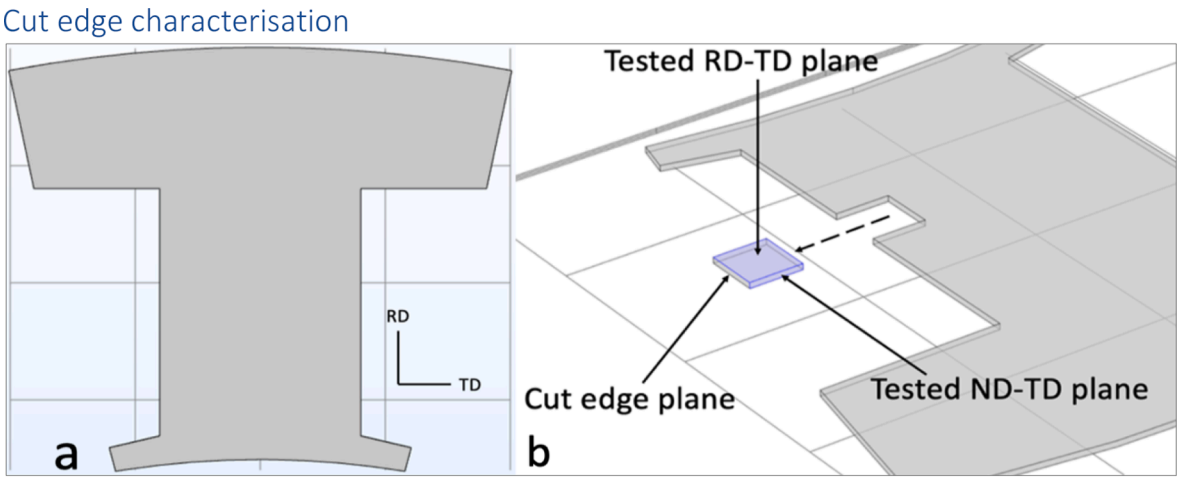

Fig. 1. Schematic diagram of stator lamination chip of an electric motor (a) and tested locations of stamped cut edge (b) where RD is rolling direction, TD is transverse direction and ND is normal direction.

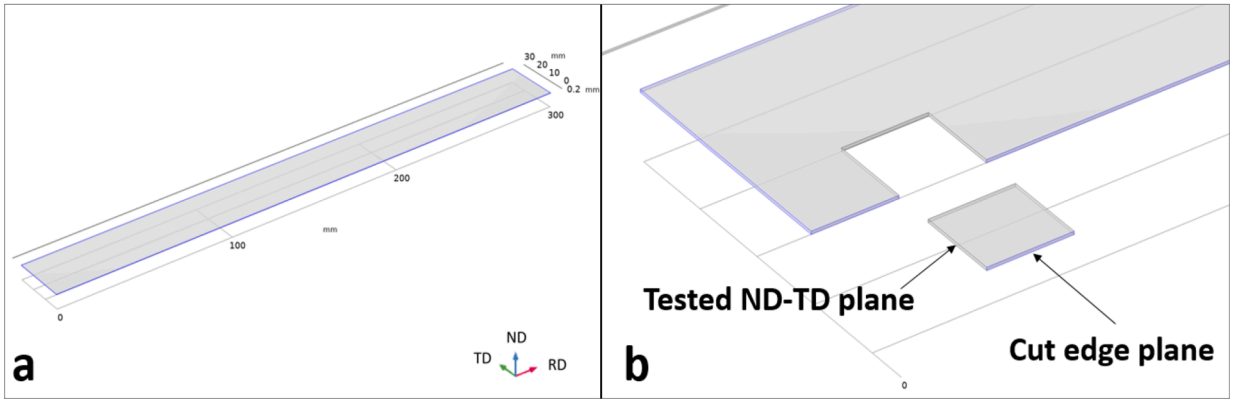

Fig. 2. Schematic diagram of SST sample (a) and tested locations of guillotine cut edge (b).

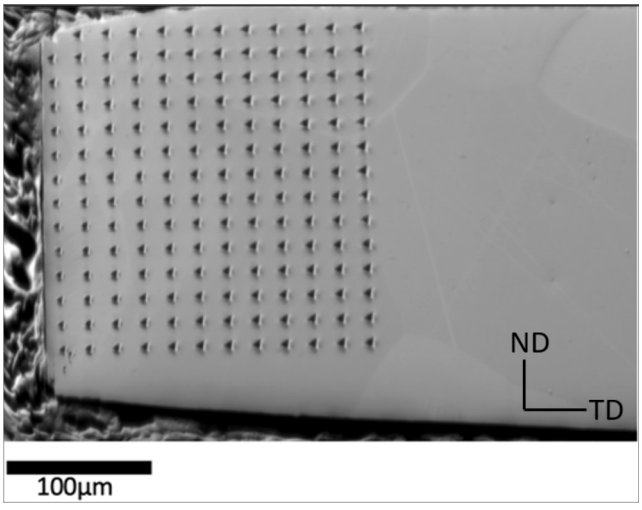

Fig. 3. Nano-indentation array placement on the ND-TD plane from the cut edge of a lamination.

variation of punched cut edge damage has been related to: the electrical steel's grain size [14] (with a smaller grain size leading to a smaller cut edge affected zone); the sharpness of the cutting tool (where a sharper tool gives less magnetic deterioration [11,13,15,16]); cutting tool

Table 1
Plastic strain level put into the sub-size ASTM E8 standard tensile samples.

Sample number	Engineering strain [%]
1	0.0
2	3.2
3	4.6
4	7.6
5	9.5
6	10.4
7	13.9
8	15.2
9	18.2

Table 2
Plastic strain levels of SST testing.

Test number	Engineering strain [%]
1	0.0
2	0.8
3	2.6
4	3.2
5	4.6
6	7.2
7	12.0
8	13.4
9	14.8
10	17.0

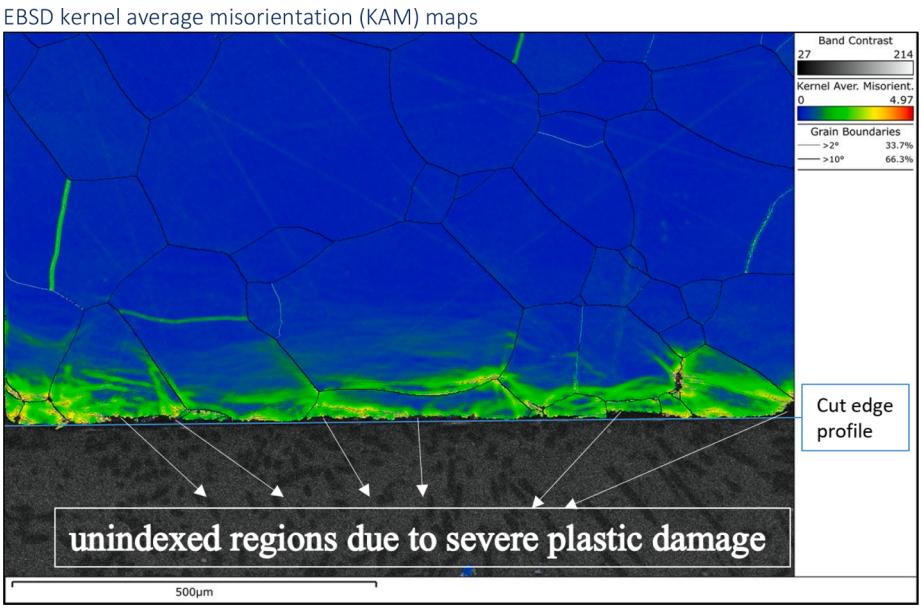

Fig. 4. KAM map of the stamped cut edge of the stamped lamination sample on the RD-TD plane.

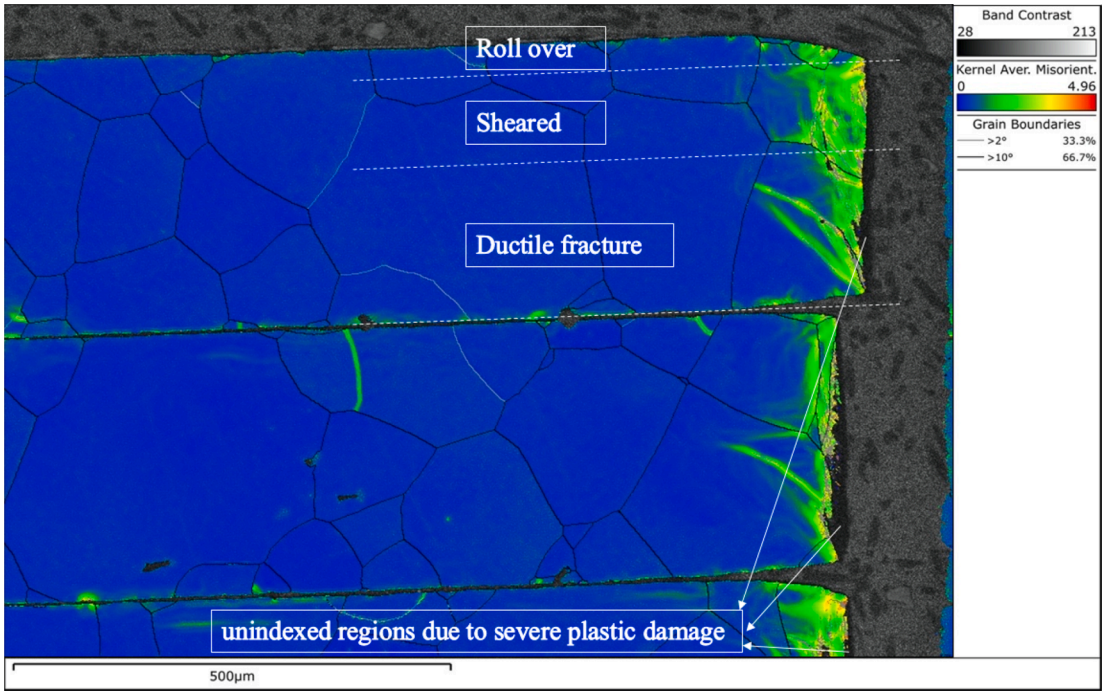

Fig. 5. KAM of the stamped cut edge of the stamped lamination sample on the ND-TD plane (multiple samples stacked together).

clearance and cutting velocity (smaller clearance and lower velocity giving less cut edge effect on magnetic deterioration [16,17]); and the hardness and thickness of the lamination (damage is greater in softer and thicker materials [18]). Nano-indentation and micro hardness studies are used to quantify the cut edge damage severity and width, with decreasing hardness values from the edge to between 0.1 mm and 1 mm width reported [14,17–27]. Electron backscattered diffraction (EBSD) characterisation of misorientation angles due to plastic deformation giving damage widths between 0.2 mm and 0.4 mm has been reported [11,27]. Nano-hardness and EBSD characterisation have a resolution of less than 1 μm to several micron metres [18,28,29]. Some researchers have reported magnetic related methods of cut edge characterisation including measuring localised flux around conical holes artificially made on samples [10], Kerr microscopy [30], and magnetic needle probe measurements [12,31], giving a large range of deteriorated widths from 1.4 mm to 10 mm [10,12,30,31]. These magnetic measurements have different measurement resolutions: 0.5 mm diameter probe line measurement in [12,31], 0.15 mm by 0.2 mm area scan of Kerr microscopy [30], and conical hole separation of 1 mm in [10]. Both Weiss et al. [11] and Omura et al. [18] simulated shear cutting using an FE model to calculate the residual elastic stress distribution in the cut edge area. As both plastic deformation and elastic stress affect the magnetic property of NGO steel this may explain why magnetic measurements [10,12,30,31] quantified larger cut edge widths as both plastic strain and residual elastic stress affected the magnetic signals, however the lower resolution accuracy of these methods may also result

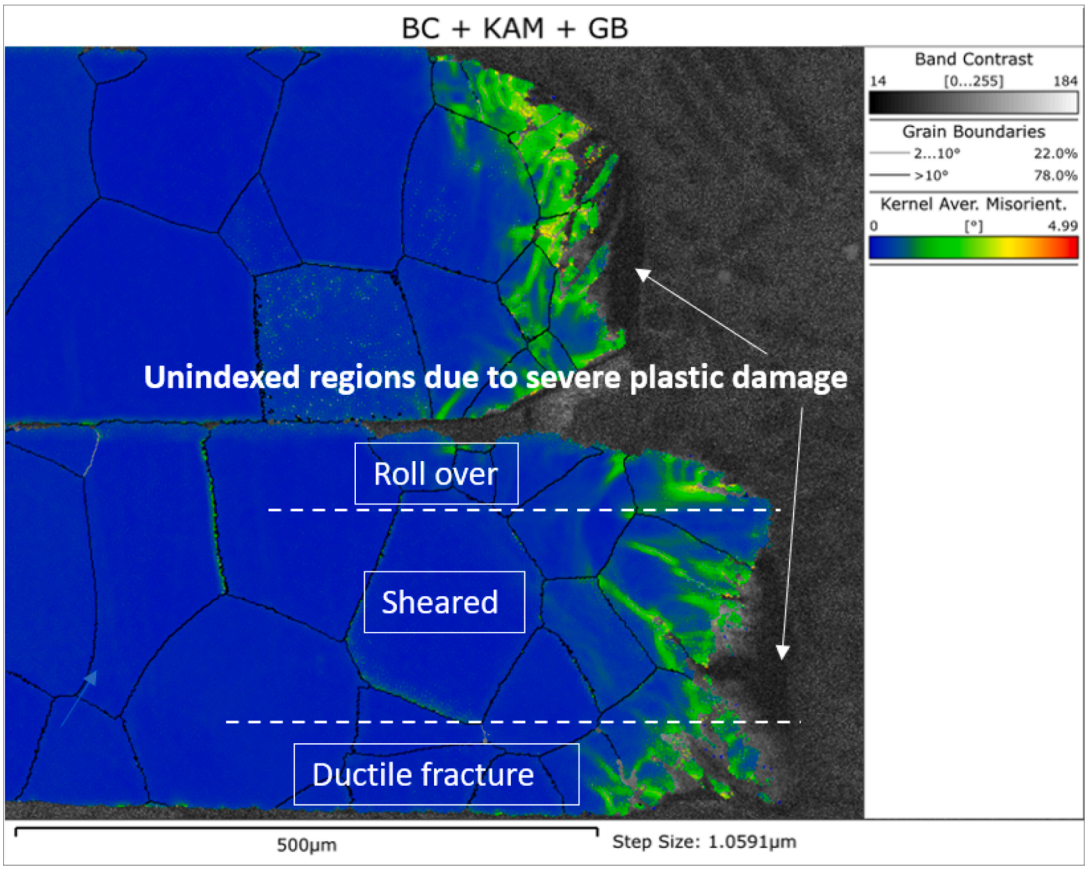

Fig. 6. KAM map of guillotine cut edges of NGO lamination on the ND-TD plane.

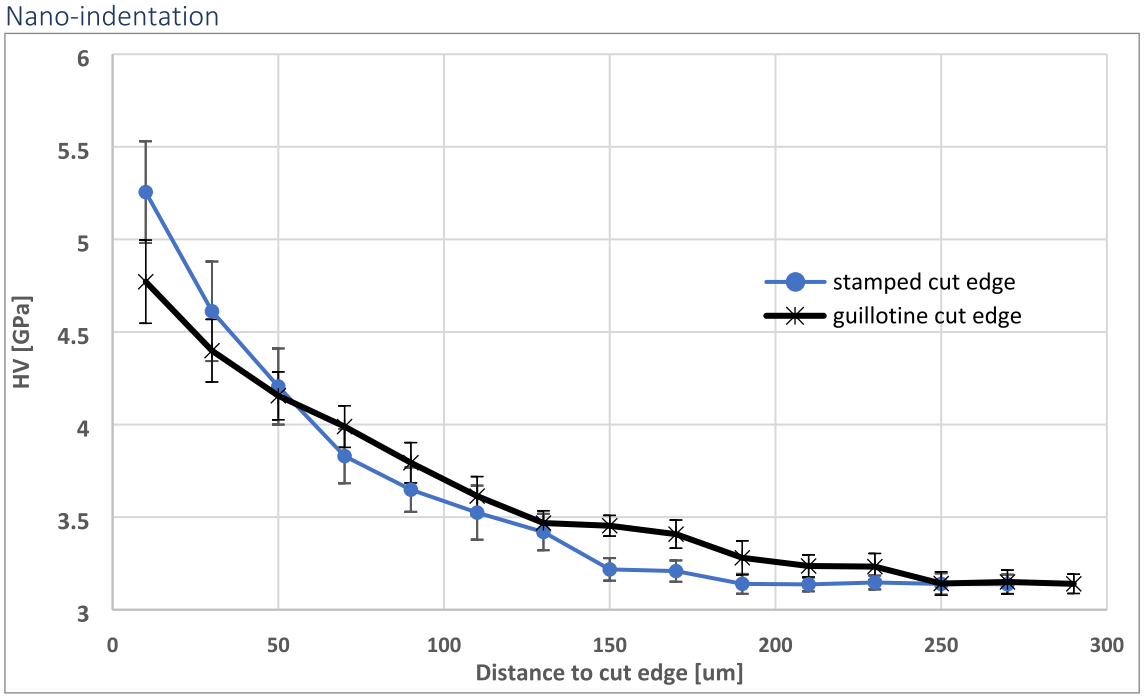

Fig. 7. Nano-indentation change from cut edge surface to the centre of the sample on the ND-TD plane.

in errors.

Cut edge damage in e-machine simulations is implemented in three ways. Firstly, via a uniform magnetic property change by adjusting the bulk magnetic properties to compensate for the cut-edge deterioration. This has been implemented in [5,32] resulting in a 15–51% iron loss increase depending on cut edge quality. Secondly, via a layered

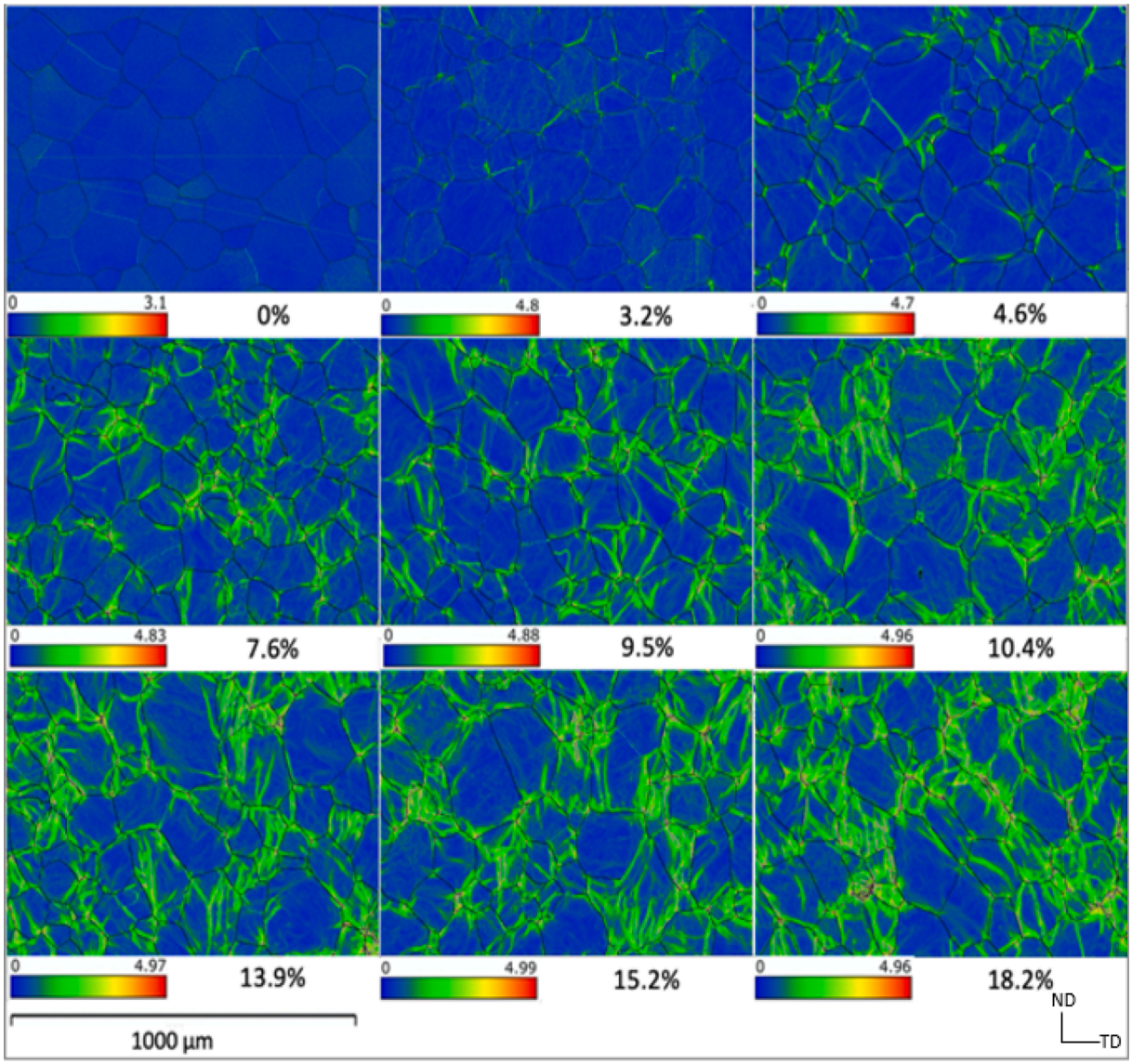

Fig. 8. EBSD local misorientation maps of sub-size ASTM E8 standard tensile samples with 0% strain to 18.2% plastic. strain.

approach [7,8,14,23,33–39], where different layers are created in the e-machine geometry close to the cut edge with the largest level of degradation given to the layer closest to the edge. The deteriorated BH behaviour is determined from measured samples with no/negligible cut edge damage and significant damage from punched edges using a Single Sheet Tester (SST) or Epstein Frame [8,14,23]. Thirdly, via an analytical function approach [18,40–42], for example, a permeability analytical function in a FE model is reported in [18,42] where the magnetic deterioration is based on a change of permeability with distance – an exponential function as used in [40,43]. However the separate effects of plastic strain and residual elastic, with the corresponding local BH behaviours, were not accounted for in the model. There have not been any reports on quantitative relationships developed between the cut edge damage type and local magnetic performance to use in layered or gradient models.

In this paper nano-indentation measurements and EBSD kernel average misorientation (KAM) values have been related to plastic strain levels in tensile test samples, tested to different plastic strain, and then used to determine the plastic strain in the cut edge damaged region for an electric motor stator lamination, all from the same grade of electrical steel. In addition, a SST has been used to measure the magnetic deterioration of the same grade of material at different plastic strain levels, and also with applied elastic stress on undamaged and plastically strained samples. These data have been used to quantitatively relate the cut edge damage to deteriorated magnetic properties in terms of anhysteretic BH changes due to pure plastic damage, a plastically strained region with residual elastic stress, and residual elastic stress only. These BH curves have been used in a three-layer 3D FEA model of SST samples for cut edge damage (plastically strained region with residual elastic stress, residual elastic stress only and undamaged region) and the model has been verified against SST measurements for strips with multiple cut edges.

2. Experimental procedure

This study characterised two different types of cut edges: commercial stamped lamination cut edge and in-house guillotine cut edge, both on the same grade NGO electrical steel (M250-35A) lamination sheet (3 wt % Si, thickness of 0.35 mm). The bulk material hardness was characterised using an array of microhardness indents (200 g load) with average hardness determined from 100 indents. Nano-indentation measurements and EBSD KAM maps have been used to quantify the cut edge plastic damage width.

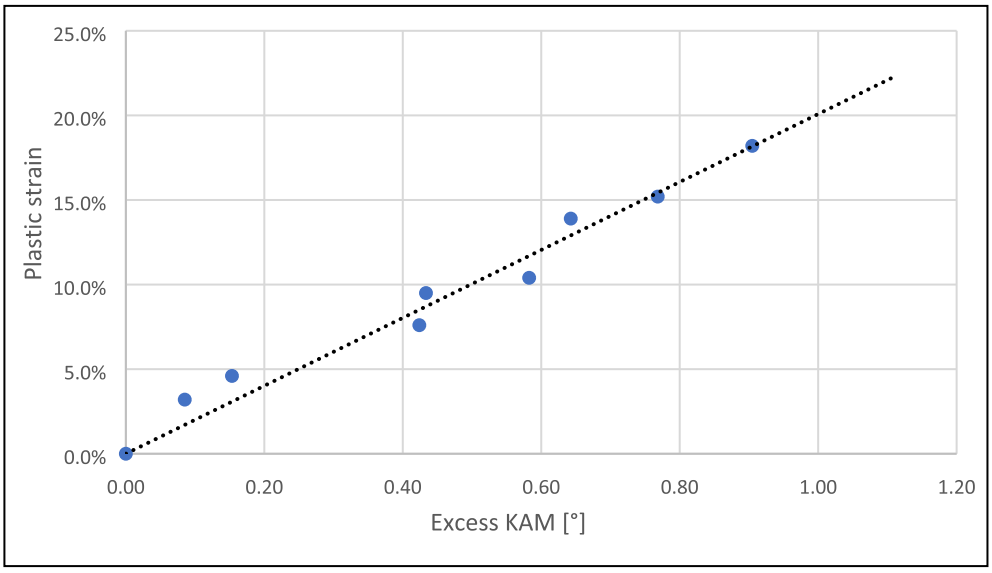

Fig. 9. Engineering strain versus excess KAM.

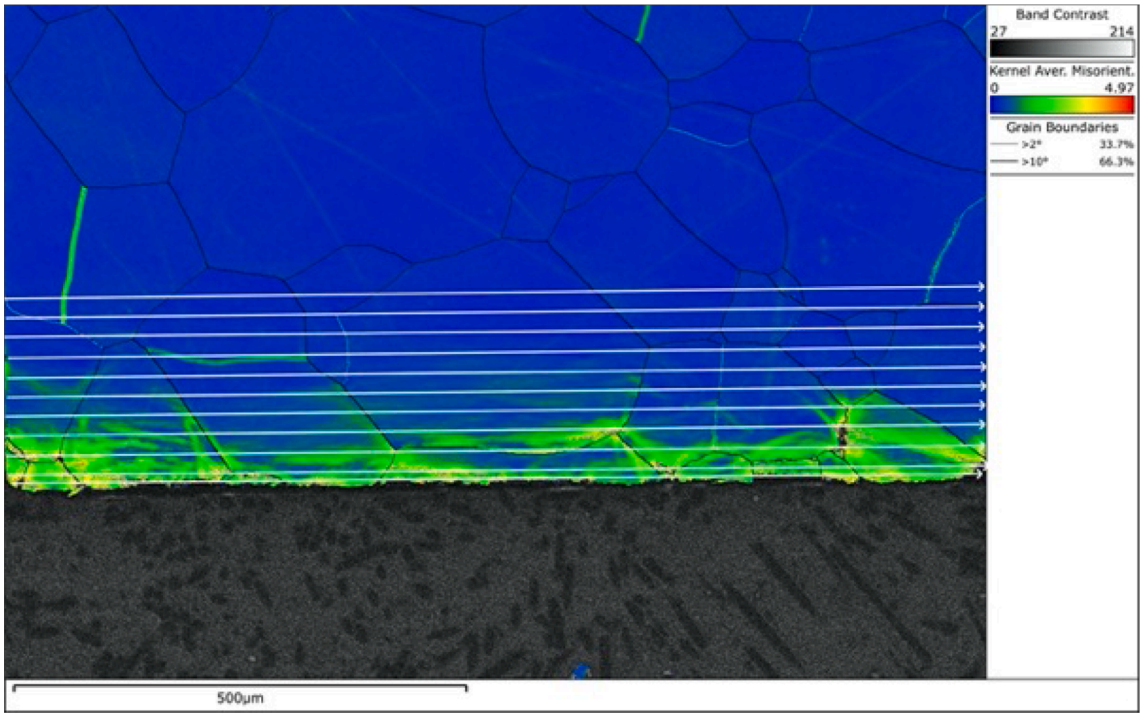

Fig. 10. Measured KAM positions of stamped cut edge, RD-TD plane.

2.1. *Cut edge characterisation*

Characterised stamped cut edge was taken from a commercial stamped stator tooth lamination as shown in Fig. 1(a). Fig. 1(b) shows the sample for characterised edge measurements, cut using a Buehler IsoMet High Speed Pro abrasive wheel cutter.

The characterised guillotine cut edge was taken from one SST strip sample that has been guillotine cut from the bulk M250-35A lamination sheet, as shown in Fig. 2(a), with the sample for cut edge characterization shown in Fig. 2(b), cut using a Buehler IsoMet High Speed Pro abrasive wheel cutter. The cut edge samples were mounted and polished to 0.06 µm surface finishing level. EBSD scans were carried out in a JEOL 7800F SEM and KAM maps were generated via Oxford Instrument Aztech Crystal software. A scanning step size of 1.06 µm was used to scan both the RD-TD plane and ND-TD plane of the cut samples.

Nano-indentation measurements were carried out over the cut edge (ND-TD plane) using a Nano Test™ Xtreme system with a Berkovich indenter. For each test cycle: the loading force was 100 mN; loading time was 30 s, holding time was 10 s, and unloading time was 30 s. An EBSD forward scanning detector (FSD) image of the indentation array in the ND-TD plane is shown in Fig. 3. According to [44], a minimum indent spacing of 10 times the indentation depth must be used to generate valid hardness values from the edge. Therefore, the first row of indentations was positioned about 10 µm from the cut edge as the indentation depth is less than 1 µm. The size (edge length) of the indent is about 3 µm, therefore the distance between the adjacent indentations was set to 20

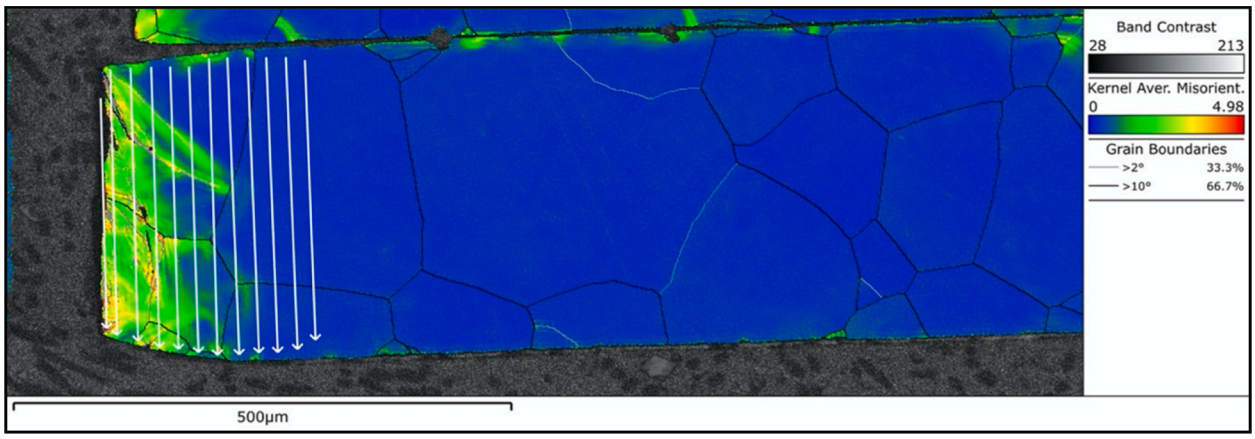

Fig. 11. Measured KAM positions for the stamped cut edge, ND-TD plane.

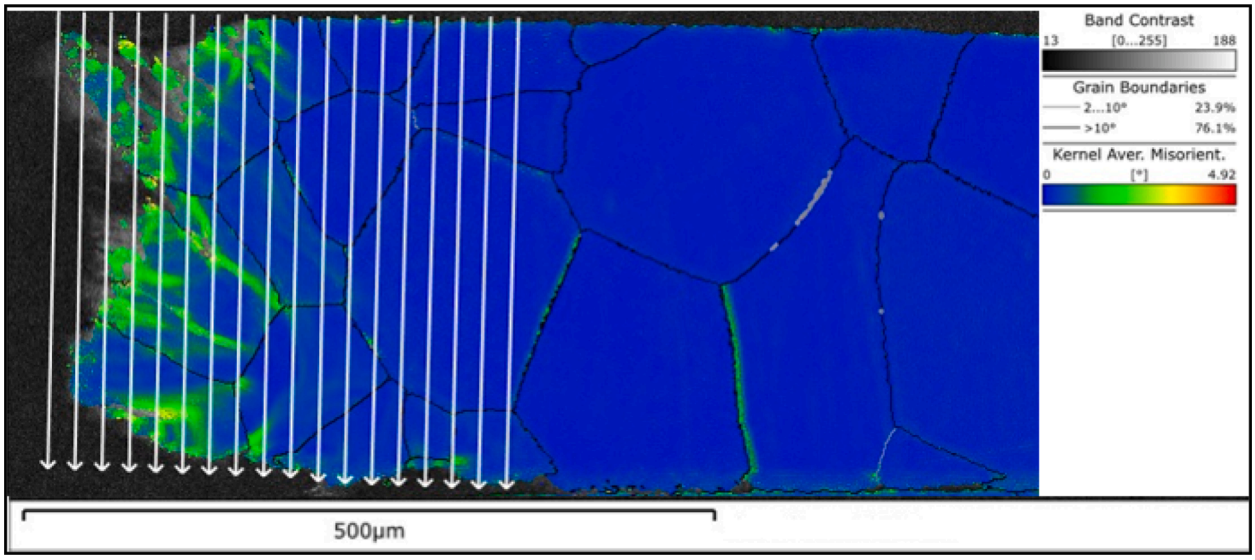

Fig. 12. Measured KAM positions for the guillotine cut edge, ND-TD plane.

µm in both the ND and TD directions to avoid neighbouring indent effects. Average nano-indentation values for every vertical line of the array were calculated to compare the hardness change from the cut edge surface into the sample.

2.2. Part 2: Assigning plastic strain values to cut edge damage

In order to relate the nano-indentation values and KAM values to quantitative plastic strain levels, nine sub-size ASTM E8 tensile samples [45] were prepared using EDM cutting from M250-35A grade electrical steel. The samples were tensile tested in a Phoenix 5 kN electro-thermal mechanical testing machine to different strain levels and the engineering strain was recorded by a strain gauge, as shown in Table 1. The engineering strain was also determined after the test pieces were unloaded by measuring the samples using an Epsilon 3448-025M-050 extensometer. After tensile testing, 6 mm square samples were cut out with a Buehler IsoMet High Speed Pro abrasive wheel cutter from the uniformly deformed region of the sample gauge length and prepared for EBSD characterisation and nano-indentation testing, using the same methodology as for the lamination sample characterisation. The indentation array used was 20 by 10 with a larger indent spacing of 150 µm to average measurements over a larger area and greater number of grains (material grain size of 130 µm) to avoid any effect of strain inhomogeneity.

2.3. Part 3: Magnetic measurements

The magnetic performance of M250-35A NGO electrical steel at different plastic strain levels, and elastic stress levels (on undamaged and plastically damaged samples) were tested using the SST with tensile function. SST strip samples (dimensions 30 * 300 * 0.35 mm) in the rolling direction were EDM cut to minimise any mechanical cut edge effect. The SST strip was initially measured in the as-received (undeformed) state at 1.5 T polarisation and 50 Hz, then a series of elastic tensile and compressive stresses were applied and magnetic properties measured. To relate magnetic performance to plastic strain and plastic strain with elastic stress, measurements were made on one SST strip incrementally strained to different plastic strain levels: the strip was tensile tested to a defined extension, equating to the desired plastic strain, given in Table 2, then the load was removed and magnetic performance measured. At each level of plastic strain, the effect of elastic stress was also assessed.

3. Results and discussion

3.1. Part 1: Cut edge characterisation

3.1.1. EBSD kernel average misorientation (KAM) maps

Figs. 4 and 5 are EBSD KAM maps of the lamination cut edge area

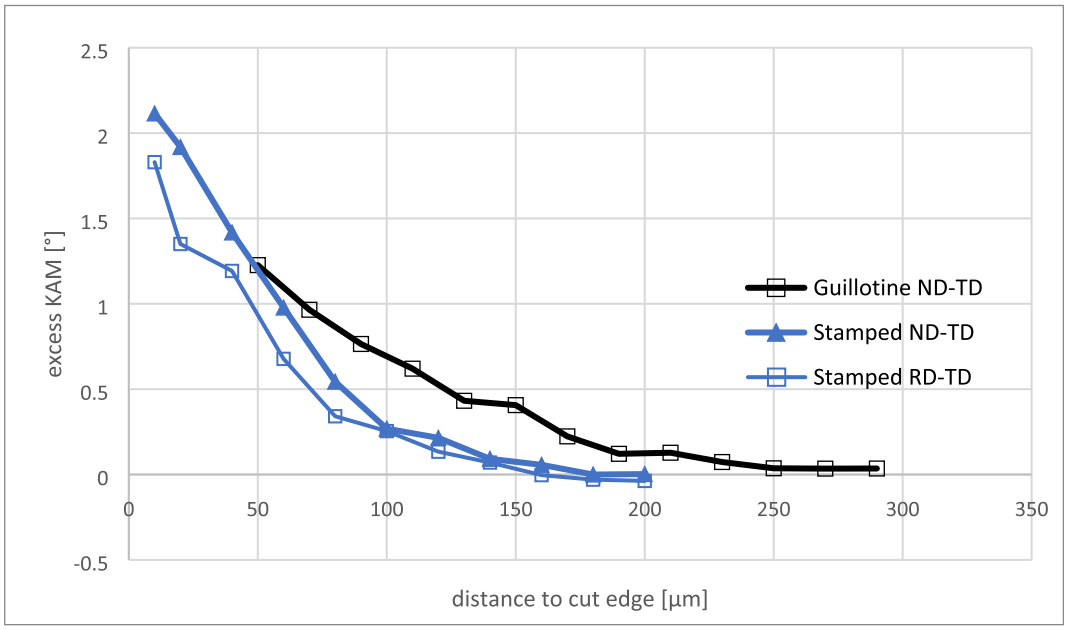

Fig. 13. Excess KAM from the sample edge on both the RD-TD plane and ND-TD plane for the stamped edge sample and on the ND-TD plane for the guillotine edge sample.

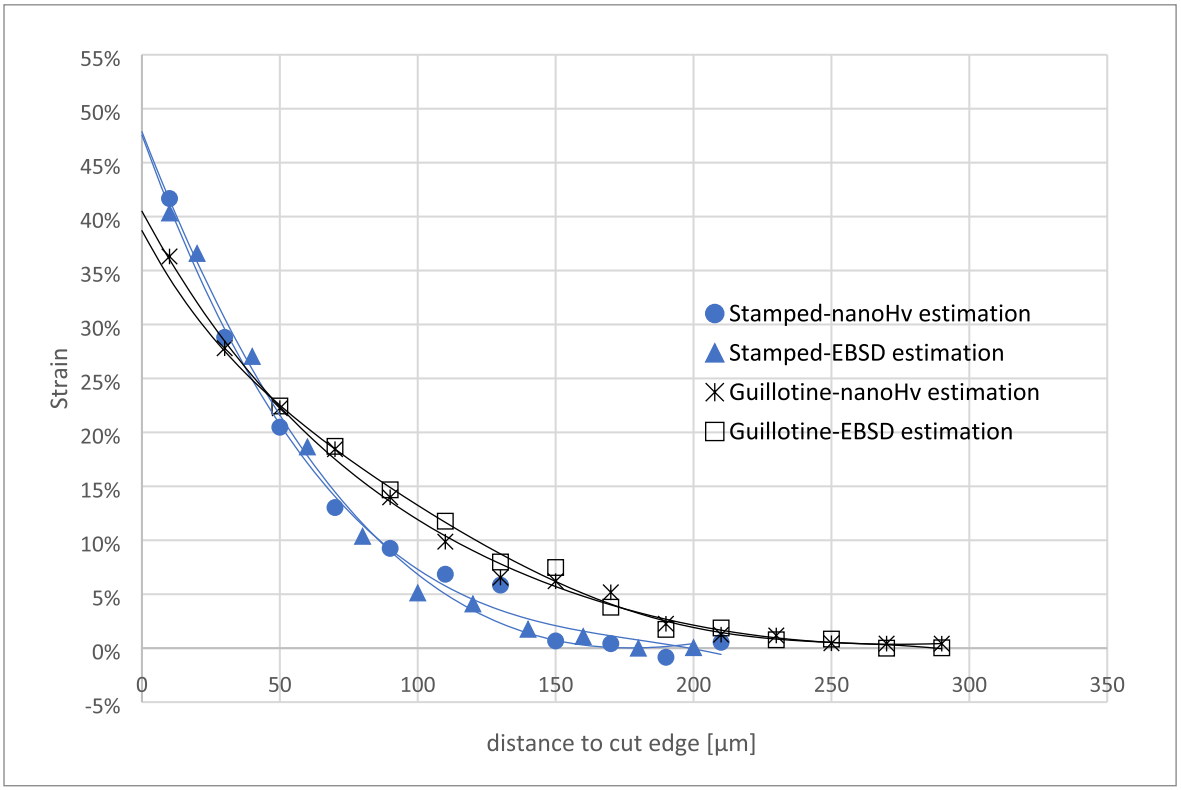

Fig. 14. Estimated plastic strain with respect to the cut edge for the stamped and guillotined samples.

indicated in Fig. 1(b). The KAM values have been determined from the 5 × 5 neighbouring EBSD pixels, where the KAM is the arithmetic mean of scaler misorientation values between groups of EBSD indexing pixels of neighbouring points (in this case taken as between the neighbouring 25 pixels). The black regions in Figs. 4 and 5 indicate the sample edge – due to the high strain and distortion at the very edge of the sample the EBSD map has unindexed points. Misorientation is estimated by comparing the neighbouring misorientation pixels from the EBSD indexing [46], so a higher misorientation angle represents a higher plastic deformation region on the local misorientation map due to the crystal lattice curvature attributed to the geometrically necessary dislocations [46–50]. In Figs. 4 and 5, the maximum distance between the edge of the sample (black region) and the place where the misorientation is consistent with the bulk of the sample is about 180 μm. Thus, the KAM maps show a damaged cut edge width of about 180 μm, which is similar to that reported for EBSD characterization of a punched edge in electrical steel

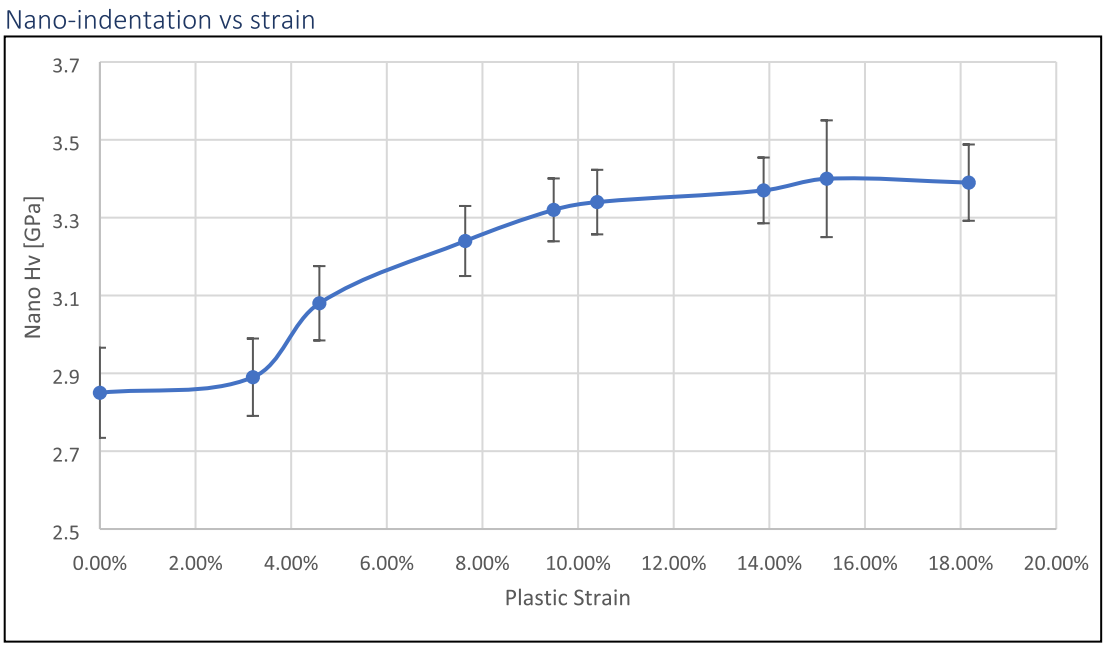

Fig. 15. Nano-indentation values of sub-size ASTM E8 standard tensile tested samples on RD-TD plane.

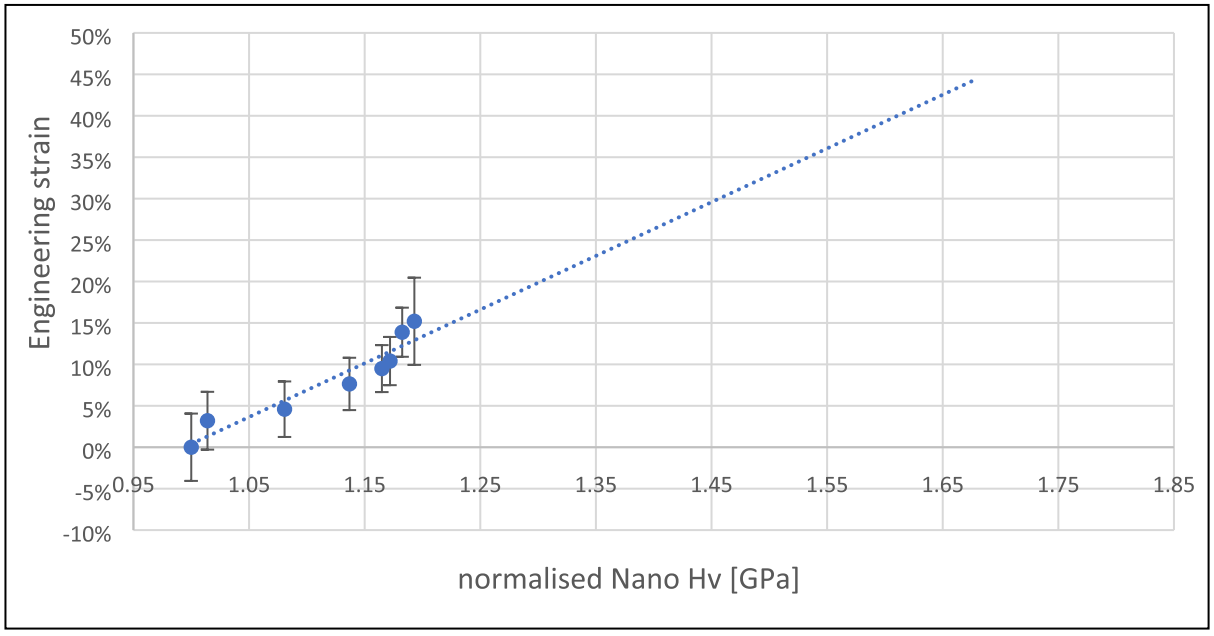

Fig. 16. Plastic Strain versus normalised nano-indentation values.

[19,28,51,52]. It has been reported that there is variation in deformation through thickness after punching [26] reflecting three deformation modes: roll over section at the top of the cut; sheared section in the middle and ductile fracture at the bottom. Some variation in misorientation through thickness can be seen in Fig. 5 (roll over at the top and ductile fracture at bottom for the orientation of the laminations shown) but there is also an effect of local grain size. The misorientation values have been averaged through thickness to consider this variability.

Fig. 6 is the KAM map of the guillotine cut edges, where the roll over, sheared, and ductile fracture regions were identified. The maximum distance between the edge of the sample (black region) and consistent misorientation region of the bulk of the sample is about 250 μm. Thus, the guillotine cut edge has a plastic deformation region of 250 μm, which is larger than a stamped cut edge.

3.1.2. *Nano-indentation*

The nano-indentation change with distance from the cut edge surface is plotted in Fig. 7. Each point in Fig. 7 represents the average value of the nano-indentation values of the corresponding vertical indentation row from the array shown in Fig. 2. As shown in Fig. 7, the nano-indentation values for the stamped cut edge decrease from 5.25 GPa to 3.14 GPa within the first 150 μm from the sample edge; then the nano-indentation values are reasonably consistent at around 3.14 GPa from 170 μm into the bulk of the sample. A higher dislocation density, associated with greater plastic deformation from cutting damage, results in a higher hardness value. Therefore, from Fig. 7, it can be concluded that the end of the damaged zone of the stamped cut edge is between 150 μm and 190 μm, which is similar to with the microhardness measured cut edge damage reported in [18] for a stamped lamination and agrees with

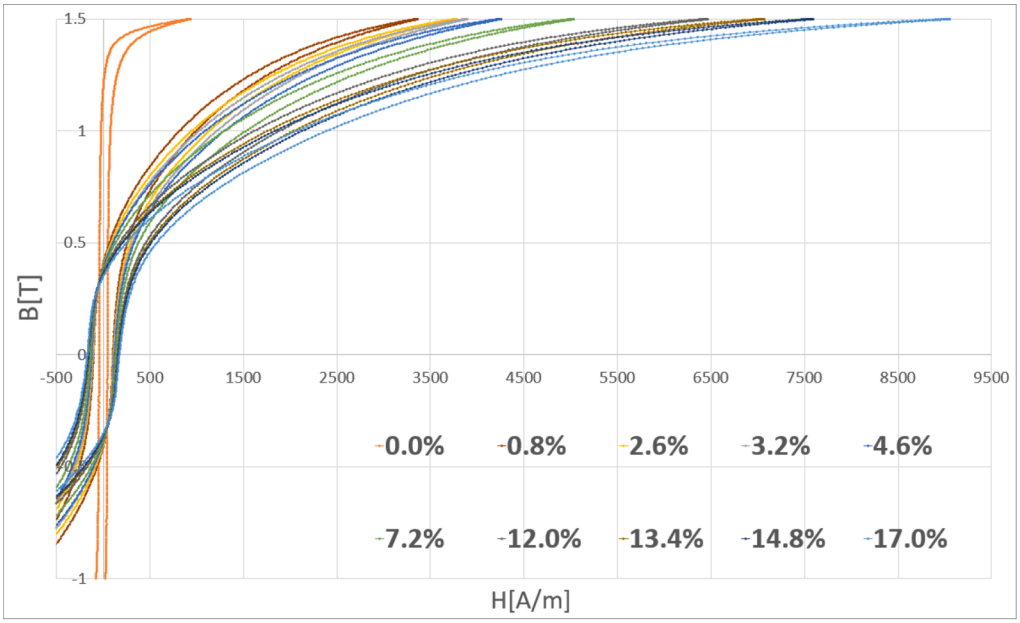

Fig. 17. SST measurements of the BH change due to plastic strain (B = 1.5 T, f = 50 Hz).

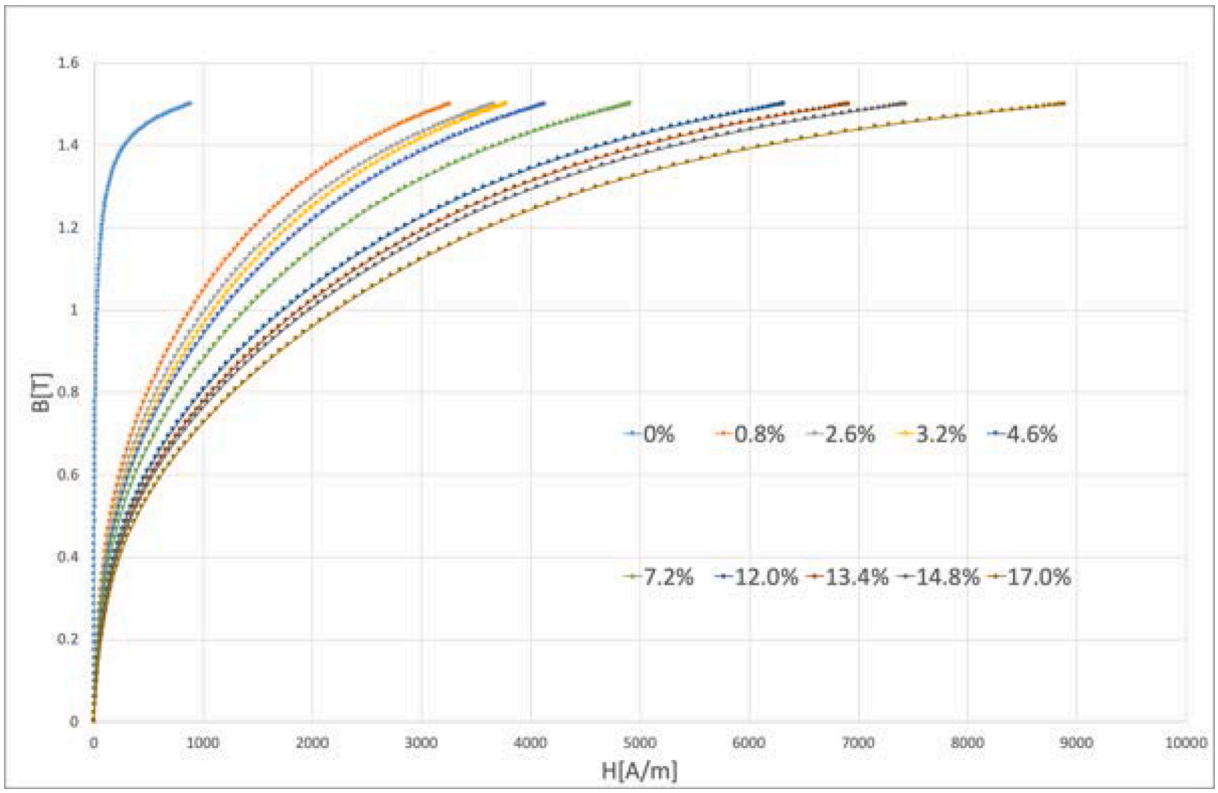

Fig. 18. Change of anhysteretic BH curve with increasing plastic strain (B = 1.5 T, f = 50 Hz).

the results obtained from the EBSD local misorientation maps for the width of the damage zone. In Fig. 7, the nano-indentation values for the guillotine cut edge decrease from 4.77 GPa to the bulk material hardness of 3.14 GPa at 250 μm from the sample edge, which is same distance as the EBSD characterised value. The standard deviation values are larger near the cut edge than in the bulk of the material, due to the through thickness variation in the roll over section, sheared section, and ductile fracture section. In the first 50 μm from the sample edge the nano-indentation values for the guillotine cut edge are lower than the stamped cut edge.

3.2. Part 2: Assigning plastic strain level to cut edge damage

3.2.1. KAM vs strain

Fig. 8 shows the increase in KAM indexing in the EBSD images for samples that were tensile tested to different plastic strain levels representing an increase in the dislocation densities, which can be seen to occur preferentially around the grain boundaries. At the higher strain

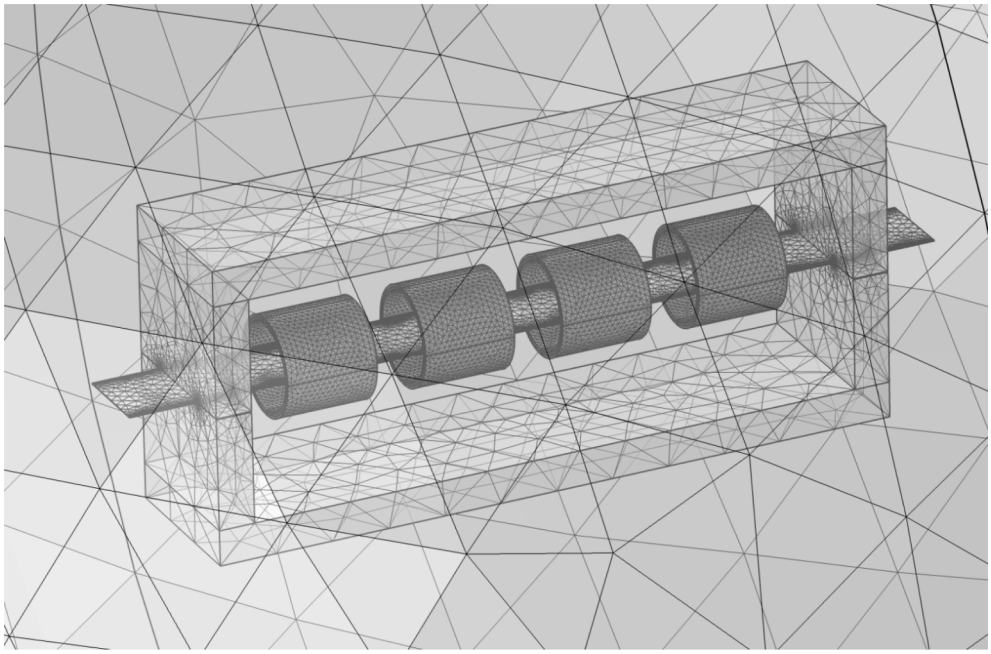

Fig. 19. FE model of SST in COMSOL (example shown of a sample with 2 guillotine cut edges).

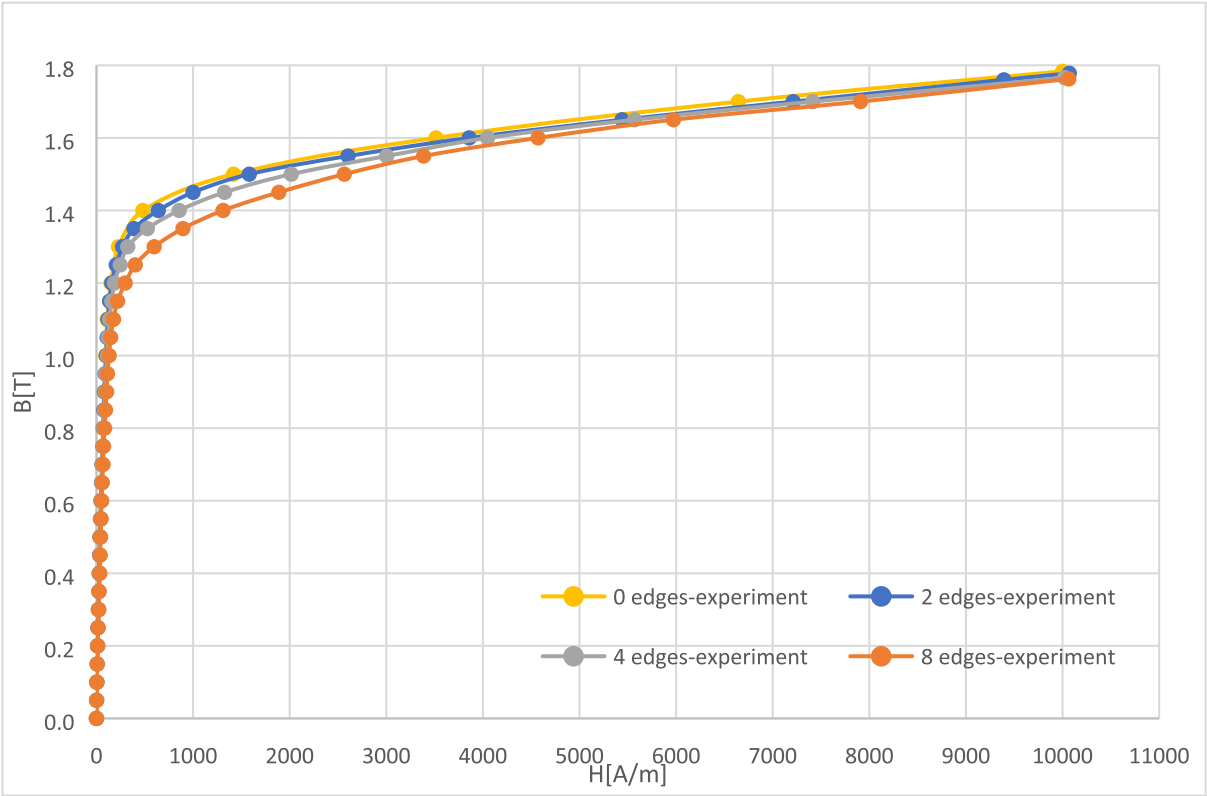

Fig. 20. Change of anhysteretic BH curves with increasing guillotine cut edges (f = 50 Hz).

level, >9.5%, higher KAM values are also observed in the interior of most grains. It should be noted that whilst a uniform elongation and macroscopic plastic strain was applied to the tensile samples, at a microstructural level the accumulation of dislocations is inhomogeneous with higher dislocation densities locally in grains oriented for easy slip and particularly at the grain boundaries. The width of the grain boundary high misorientation regions increases with an increase in applied plastic strain. The average KAM values have been determined for each plastic strain level. An 'excess KAM' has been determined, which is the increased KAM for the strained samples minus the KAM of undeformed material, thus related to dislocation density rather than sample preparation. The excess KAM values for the different applied plastic strain levels in the tensile samples are shown in Fig. 9.

The maximum uniform plastic strain that could be applied during

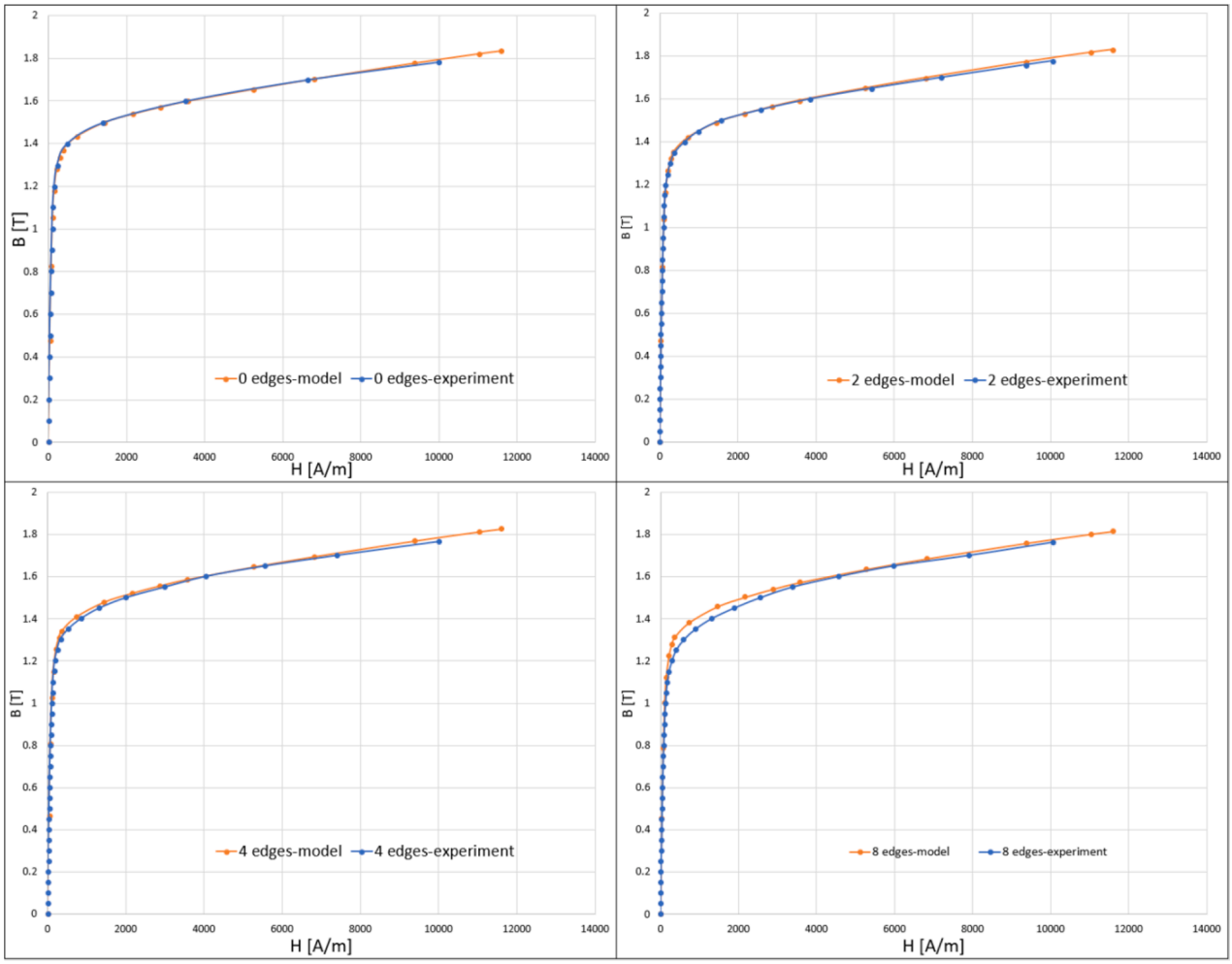

Fig. 21. SST experimental results versus COMSOL SST modelling results for 0, 2, 4, and 8 cut edges (each cut edge was represented as one plastically deformed layer).

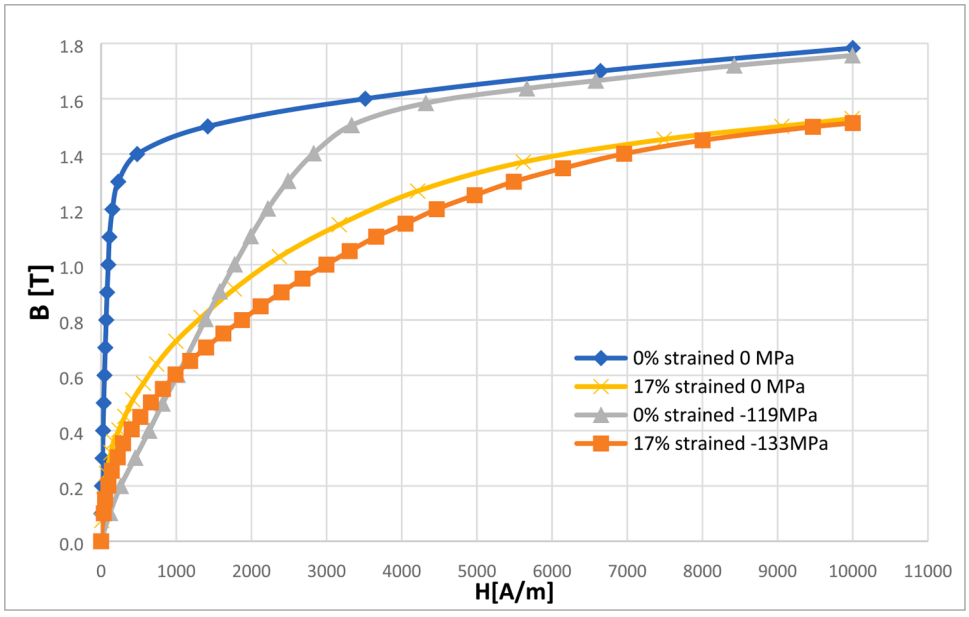

Fig. 22. Experimentally measured anhysteretic BH curves used as representative material property inputs considering the effect of elastic stress on 17% plastically strained electrical steel.

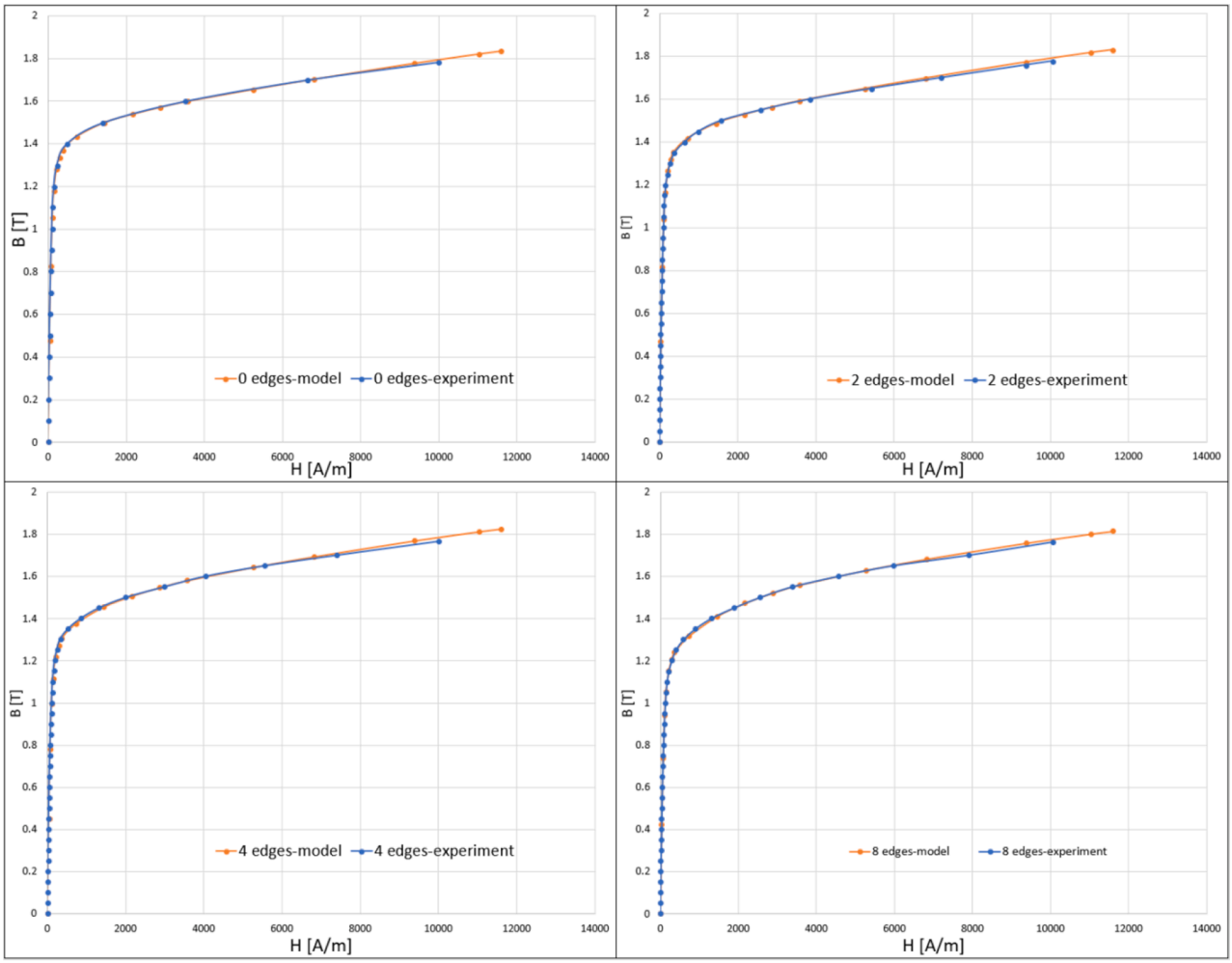

Fig. 23. SST experimental results versus COMSOL SST modelling results for 0, 2, 4, and 8 cut edges (each cut edge was represented by a plastic deformed + elastic residual stress layer and a residual elastic stress layer).

tensile testing was 18% before necking. However, the cut edge damage can result in a higher local strain, for example due to local shear, with maximum effective plastic strain of 40–50% being reported from FEM analysis at the cut edge for a 0.35 mm thick electrical steel sample [18]. The relationship between plastic strain and corresponding excess KAM was established, as shown in Fig. 9, with a linear relationship observed allowing extrapolation to higher strain value, assuming continued dislocation density increase (i.e., no recovery).

To predict the plastic strain imposed at the edge by stamping and guillotining, the KAM starting at 10 μm from the cut edge into the bulk of the material were measured every 20 μm vertical slice. The locations of the measured KAM values on both the RD-TD plane and ND-TD plane of the stamped edge are shown in Figs. 10 and 11. The locations of the measured KAM values on the ND-TD plane for the guillotine edge are shown in Fig. 12. The averaged KAM values at each location for stamped and guillotine cut edges are summarised in Fig. 13.

As seen in Fig. 13, the excess KAM on the ND-TD plane is slightly higher than the RD-TD plane close to the sample edge, which is because the strain distribution is not uniform through thickness from the roll over, shear and fracture zones. Therefore, the excess KAM from the RD-TD plane is not optimum to represent cut edge damage. Since the ND-TD plane can be used to obtain the average damage through thickness, the excess KAM from the ND-TD plane has been used to characterise cut edge damage. Figs. 9 and 13 have been used to determine the plastic strain with distance from the sample edge according to the EBSD scan on the ND-TD plane. The estimated plastic strain from EBSD at the stamped edge is in the range 45–50%, as presented in Fig. 14. The FEM predicted effective plastic strain at the cut edge in [18] is 45–50% for a similar thickness and hardness electrical steel. As shown in Fig. 14, the estimated plastic strain from EBSD at the guillotine edge is about 35–40%, which is slightly lower than for the stamped cut edge.

3.2.2. *Nano-indentation vs strain*

The nano-indentation values for the different plastically strained sub-size ASTM E8 samples have also been measured and are plotted in Fig. 15. Samples with higher plastic strain have a higher nano-indentation value, as expected. A complication when developing a relationship between nano-indentation values and plastic strain is that variations in surface preparation can lead to differences in nano-indentation values due to the work hardened layers produced by polishing [53] and/or surface oxidation. Work hardening effects will be larger for the as-received soft samples, whilst oxidation can be minimised by preparing sample just before testing, and may be the reason for the bulk nano-indentation in the cut edge sample in Fig. 7 (3.14 GPa) being different to the bulk nano-indentation in the undeformed tensile sample in Fig. 15 (2.85 GPa), despite nominally the same sample preparation and time between polishing and hardness testing being used. To assign plastic strain to the nano-indentation values, all the strained and unstrained tensile samples were mounted and polished together. All the strained nano-indentation data were normalised to the zero deformed sample, Fig. 16, which then gives an approximately linear relationship between the plastic strains applied and normalised nano-

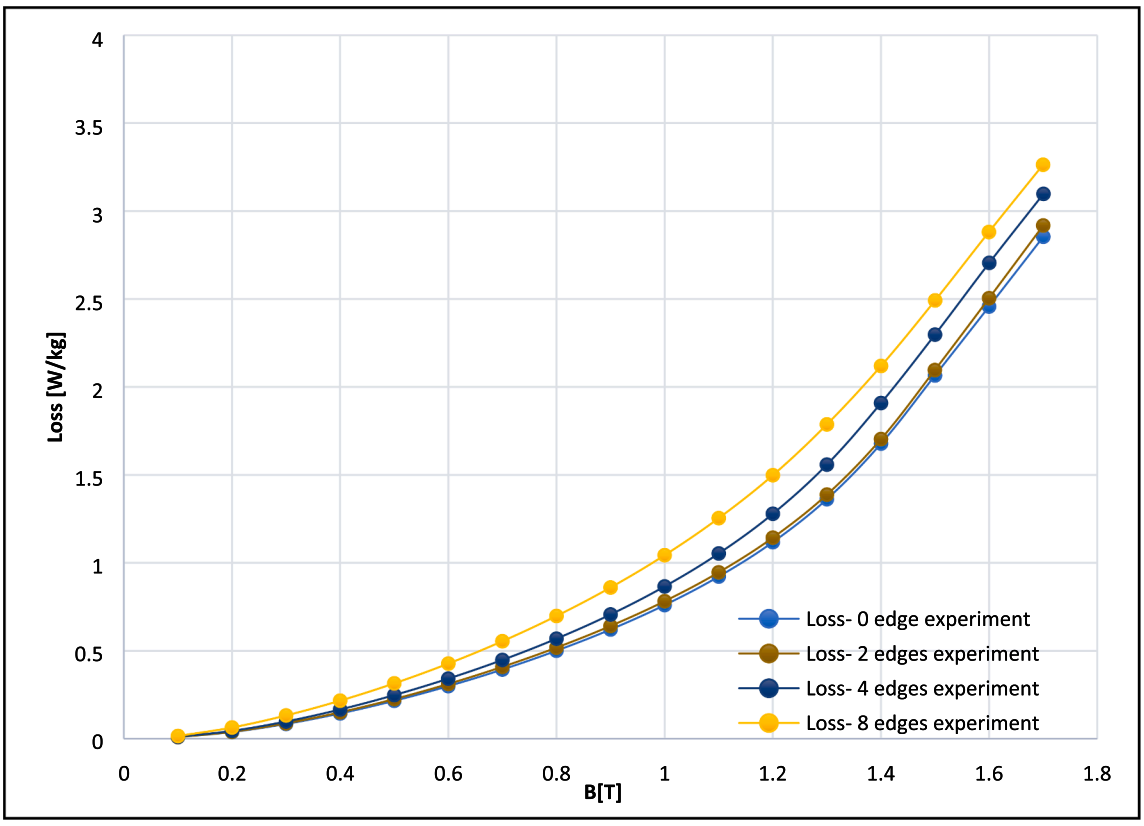

Fig. 24. Measured specific iron loss vs flux density curves of SST samples with increasing guillotine cut edges (f = 50 Hz).

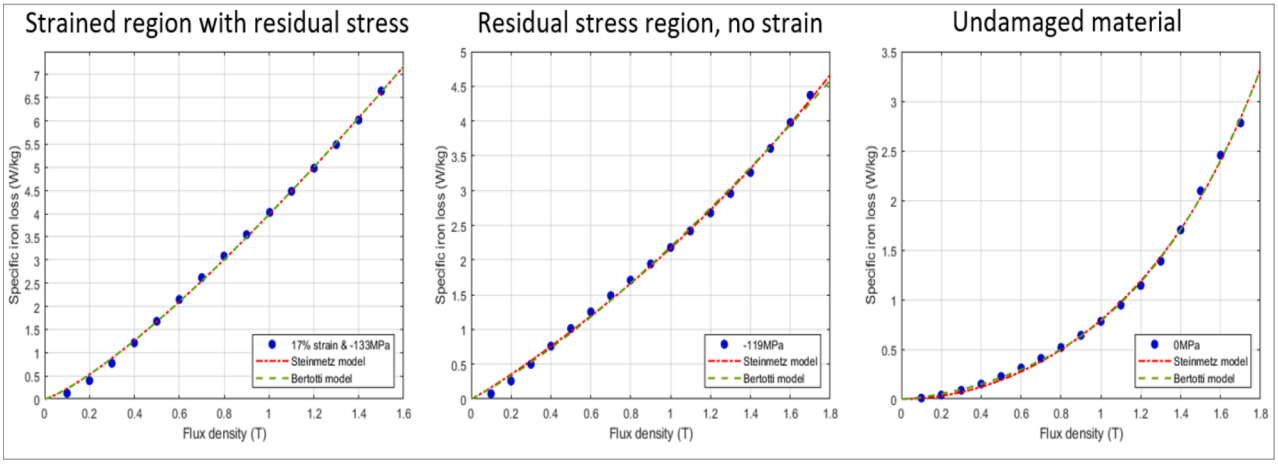

Fig. 25. Specific iron loss vs flux density curves.

indentation value. This relationship is expected (assuming no recovery) as the dislocation density increases in the sample. From Fig. 16 the estimated strain values can be obtained for the normalised nano-indentation values measured for the cut edge region, shown in Fig. 14 along with the EBSD data. The maximum strain predicted at the lamination cut edge is in the range 40–50%. As shown in Fig. 14, the strain values estimated for both the stamped and guillotine cut edge from the EBSD KAM maps and by nano-indentation are very similar.

3.3. Part 3: Magnetic performance variation at different plastic strain levels

SST strips were tensile tested to different strain levels, as shown in Table 2, and the full BH curves were measured at 50 Hz frequency and 1.5 T polarisation and are plotted in Fig. 17. The BH curves start to rotate clockwise when plastic deformation is introduced, as has been reported previously [20,54–60].

The full BH curves were converted to anhysteretic BH curves as the appropriate format for use in the COMSOL multi-physics SST model, shown in Fig. 18. The anhysteretic BH curves were calculated by averaging the two applied field values (H) at each polarisation (B) value and only positive B was used as the full BH curve is symmetrical.

3.4. FE modelling for cut edge effect on magnetic deterioration

An SST finite element (FE) model was constructed using COMSOL

Table 3
Steinmetz and Berttoti coefficients for loss calculation.

Steinmetz: $Ps = K_h \times f \times B^{(alpha+beta\times B)} + 19.7391 \times k_e \times f^2 \times B^2$

Loss coefficients	Plastic with stress region (−133 MPa)	Residual stress region (−199 Mpa)	Undamaged material
K_h	7.96E−02	4.34E−02	7.04E−04
alpha	1.25E+00	1.11E+00	5.44E+00
beta	2.22E−14	1.09E−01	3.68E−04
k_e	2.25E−14	2.45E−14	1.54E−05

Bertotti : $Ps = K_h \times f \times B^{(alpha)} + 2.2617E-06 \times f^2 \times B^2 + K_{exc} \times f^{1.5} \times B^{1.5}$

Loss coefficients	Plastic with stress region(−133 MPa)	Residual stress region (−199 Mpa)	Undamaged material
K_h	7.95E−02	2.09E−02	4.38E−03
alpha	1.25E+00	9.33E−01	3.71E+00
K_{exc}	2.34E−13	3.23E−03	1.59E−03

Multiphysics software with the dimensions and details of the experimental setup of the Brockhaus SST system. As shown in Fig. 19, the NGO SST sample is placed between the upper and lower yokes, and a layered approach was used for considering the cut edge; there are 4 groups of 50-turn exciting coils with 50-turn sensing coils underneath. The model was constructed in the magnetic fields-time domain to simulate an AC magnetic scenario with 50 Hz frequency. The whole setup was built within an air ball of 600 mm radius. Excitation coils were defined as numeric homogenized multi-turn coils with current input obtained from the SST experimental data. Multiple mesh level method was applied to optimise the simulation time. As NGO SST sample and cut edge regions were the most cared in this model, the finest meshes were performed in those domains (maximum domain size of 0.4 mm and minimum domain size of 0.01 mm). The complete mesh consists of 1,085,937 domain elements, 167,620 boundaries, and 32,546 edge elements. The material property of the NGO SST sample was defined under Ampere's Law using the interpolation anhysteretic BH curve in Fig. 18. The cobalt iron yokes and coils were defined using the relative permeability for calculation under Ampere's Law (defined boundary condition in COMSOL). The model was adjusted for the undamaged NGO material; the input BH of undamaged material was selected and the model was adjusted until the output BH matched the input BH of the material. BH output was derived through calculating the volume averaged B and H in the sample under the coil.

Experimental data has been used to verify the SST FEM modelled effect of cut edge damage on BH magnetisation curves. Full BH curves have been measured to observe the change due to different numbers of guillotine cut edges (0, 2, 4, and 8) for SST samples where the measurement flux direction is parallel to the cut edge direction (sample width of 30 mm and magnetic path length of 224 mm). The SST sample with 0 cut edges was EDM cut as EDM has a minimal effect on magnetic properties as there is negligible edge damage [61]. The anhysteritic BH curves for the SST samples with different numbers of cut edges are plotted in Fig. 20 and show a similar trend to that reported in the literature [20], where magnetic deterioration occurs when more cut edges are introduced to the SST sample.

To model the cut edge damage effect, an assumption is made that each guillotine cut edge has a 250 μm plastically damaged width based on the characterisation work, Fig. 14. An average plastic strain of about 17.0 % in that region was calculated from Fig. 14. Therefore, the anhysteretic BH curve for 17.0% plastic strain from Fig. 18 was chosen to represent the guillotine cut edge layer material property in the model. The undamaged material BH curve in the model was assigned with experimental data for the 0 cut edge data in Fig. 20. The SST model was used to predict the BH behaviour of strips with 2, 4, and 8 cut edges and the results compared to the measured data, Fig. 21. Modelled BH outputs are less deteriorated than the measured BH data, which suggests that there is an additional factor that needs to be considered. The modelling results only consider the plastic cut edge damage; however, it has been reported that elastic residual stresses are also present after cutting. Both [11,18] reported FE modelling results for the residual elastic stress distribution in the sheared cut edge region for a similar grade and thickness electrical steel. The residual stress (both tensile and compressive elastic stresses are present) acts on the plastically deformed cut edge region and extends into the non-plastically deformed region; the total width affected by the residual elastic stress is reported to be 300–500 μm, compared to the plastic strain affected region of 220 μm. Both tensile and compressive stresses deteriorate the magnetic properties, with compressive stress being more detrimental [58]. An average elastic residual stress over the region that is also plastically deformed has been estimated to be −133 MPa by integrating the compressive stress distribution in [18] and averaging over the plastic deformation width of 250 μm. The same method was applied to estimate the average compressive residual elastic stress in the non-plastically strained region in [21] giving −119 MPa over a width of 220 μm (i.e. 250–240 μm from the sample edge).

To allow consideration of the effect of plastic damage as well as the elastic residual stress, the cut edge region was classified into two layers. First layer represents plastic damage with residual stress due to cutting (at the very edge of the material) and second layer represents residual elastic stress that spread into the non-strained material (between plastic damage region and undamaged region). A second model with two cut edge layers for each guillotine cut edge was constructed. The first layer of 250 μm represents the plastically deformed region with 133 MPa compressive elastic stress. The input anhysteretic BH curve for the first layer was measured using the 17% plastic strained sample with an applied 133 MPa elastic compressive stress: the anhysteretic BH curve is shown in Fig. 22. The second layer of 220 μm was added adjacent to the first layer to represent the region affected by residual elastic stress but no plastic strain. The representative anhysteretic BH curves were measured using non deformed material with an applied elastic compressive stress in the SST equipment, Fig. 22. Comparison between the second set of modelled anhysteretic BH curves (considering both plastic damage and residual elastic stress) with different guillotine cut edges is shown in Fig. 23. Fig. 23 shows a very good fit between the modelled anhysteretic BH curves with the experimental data showing that modelling with the two layers for plastic strain + residual elastic stress and residual elastic stress is an appropriate method to represent cut edge damage.

The specific iron loss estimation was performed using the Bertotti and Steinmetz loss equations [62] with the experimental SST data for the samples with different numbers of cut edges shown in Fig. 24. To model the total iron losses, the values for the different layers in the model need to be considered. Fig. 25 shows the specific iron loss versus flux density curves for the samples representing the different layers, i.e., with 17% strain under compressive stress of 133 MPa, compressive stress of 119 MPa only, and undamaged sample. The determined coefficients for the Steinmetz and Berttoti empirical equations are shown in Table 3. The specific iron losses of the whole SST samples in the model were calculated by summing the losses for each cut edge layer and the modelled and measured specific iron loss of SST samples with different number of cut edges were plotted in Fig. 26. There is good agreement between the measured and modelled values.

4. Conclusions

The magnitude and width of the plastic damage caused by the cut edge effect for a commercially stamped lamination and guillotined strip, both from M250-35A (3 wt% Si) grade electrical steel, were characterised with EBSD KAM maps and nano-indentation. Samples of the same steel grade were tensile tested to different plastic strain levels and analysed to determine the relationship between EBSD KAM and nano-indentation values and plastic strain. This relationship was used to

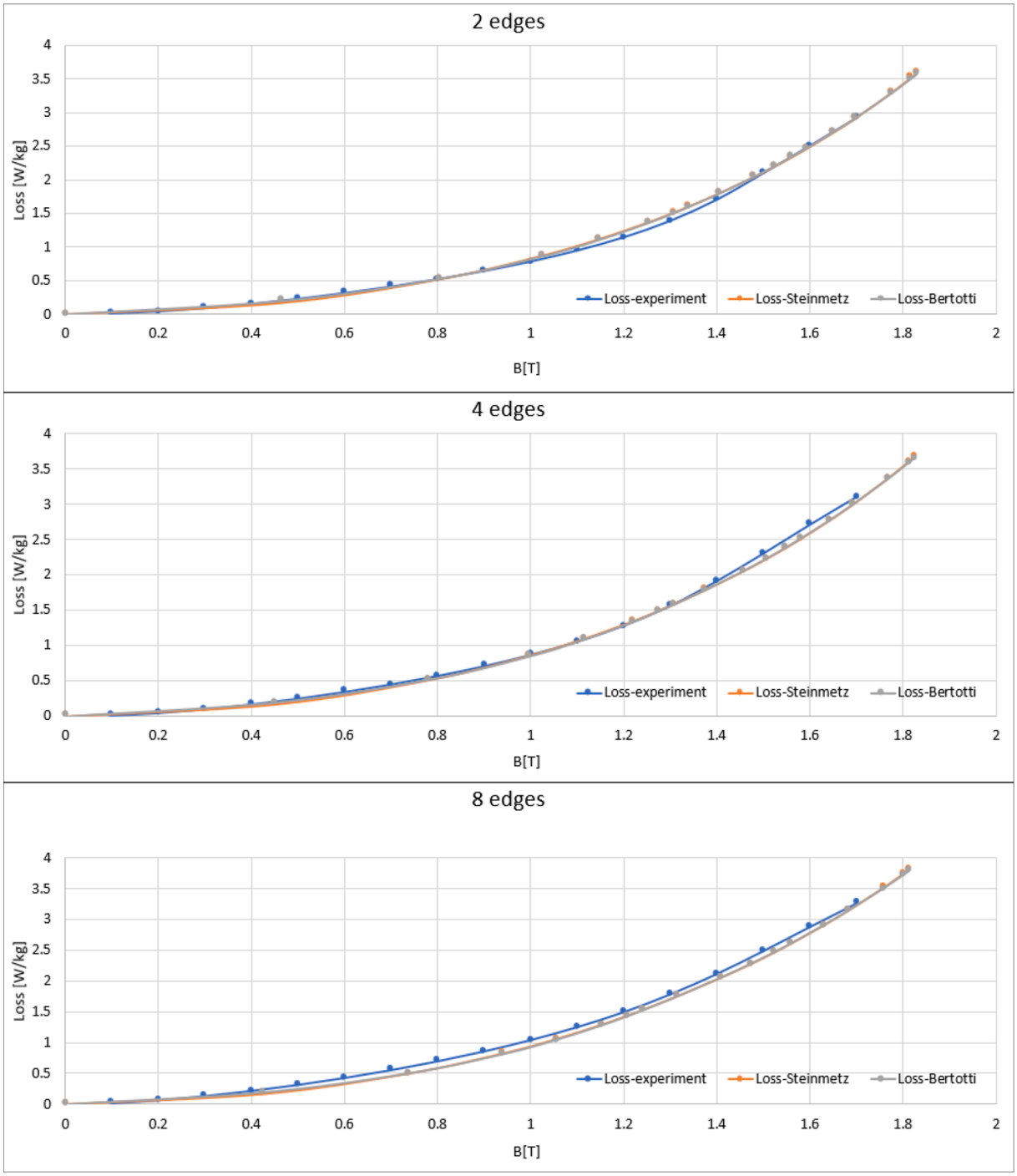

Fig. 26. Modelled (Steinmetz and Berttoti) and measured specific iron loss of SST samples with different number of cut edges.

quantify the maximum strain and damaged width for the stamped and guillotined cut edge. It was found that the EBSD and nano-indentation mapping gave the same plastic strain distribution from the cut edge with a maximum plastic strain of 45–50% at the stamped cut edge and a plastic damage width of 180 μm; the guillotined cut edge had a wider plastically damaged zone of 250 μm but slightly lower maximum strain of 35–40% at the edge.

The magnetic properties of the electrical steel were determined for the as-received condition and after the application of plastic strain, elastic stress and combined elastic stress on plastically strained samples using a SST and the corresponding anhysteretic BH curves determined.

A FEA model for the SST sample was built using COMSOL Multi-physics to model the effect of guillotine cut edge damage on magnetic performance. The cut edge damage was initially represented by a single-layer approach using an anhysteretic BH curve for the material with plastic strain of 17%, representative of the average plastic strain for the experimentally determined cut edge area. The predicted magnetic performance for samples with different numbers of cut edges (0, 2, 4, 8) was compared to experimental data and it was found that considering plastic damage only was insufficient to represent the magnetic deterioration. A two-layer model was built to include elastic stress and plastic strain at the cut edge, where SST data for samples with 17% plastic strain and 133 MPa compressive elastic stress and 133 MPa compressive elastic stress only were used for the two layers. The compressive elastic stress

level and width of the affected zone were determined from literature FE model predicted residual stress distributions for the same material and thickness [18]. The two-layer SST FE model predictions, considering residual elastic stress acting on the plastic damage region (250 μm width) and non-plastically strained region (220 μm width) were compared to the SST measured data and excellent agreement (both hysteretic BH and specific iron loss) were observed for the deteriorated magnetic behaviour due to the cut edge effect. Therefore, it is clear that both the plastic strain and elastic stress cut edge effects need to be accounted for when determining the magnetic deterioration.

Declaration of Competing Interest

The authors declare that they have no known competing financial interests or personal relationships that could have appeared to influence the work reported in this paper.

Acknowledgements

The authors would like to thank WMG, University of Warwick for providing the research facilities, and Tata Steel for supplying the materials. The authors also thanks for the support from Brockhaus equipment.

Funding

This research did not receive any specific grant from funding agencies in the public, commercial, or not-for-profit sectors.

References

[1] A. Boglietti, First approach for the iron losses building factor determination, in: Conf. Rec. – IAS Annu. Meet., IEEE Ind. Appl. Soc., vol. 1, 1999, pp. 489–493. doi: 10.1109/ias.1999.799998.
[2] N. Denis, S. Odawara, K. Fujisaki, Attempt to evaluate the building factor of a stator core in inverter-fed permanent magnet synchronous motor, IEEE Trans. Ind. Electron. 64 (3) (2017) 2424–2432, https://doi.org/10.1109/TIE.2016.2573267.
[3] Z. Gmyrek, A. Cavagnino, L. Ferraris, Estimation of the magnetic properties of the damaged area resulting from the punching process: experimental research and FEM modeling, IEEE Trans. Ind. Appl. 49 (5) (2013) 2069–2077, https://doi.org/10.1109/TIA.2013.2261041.
[4] A. Cavagnino, R. Bojoi, Z. Gmyrek, M. Lefik, Stator lamination geometry influence on the building factor of synchronous reluctance motor cores, IEEE Trans. Ind. Appl. 53 (4) (2017) 3394–3403, https://doi.org/10.1109/TIA.2017.2683439.
[5] M. Hofmann, H. Naumoski, U. Herr, H.-G. Herzog, Magnetic properties of electrical steel sheets in respect of cutting: micromagnetic analysis and macromagnetic modeling, IEEE Trans. Magn. 52 (2) (2016) 1–14, https://doi.org/10.1109/TMAG.2015.2484280.
[6] A. Schoppa, J. Schneider, J.O. Roth, Influence of the cutting process on the magnetic properties of non-oriented electrical steels, J. Magn. Magn. Mater. 215 (2000) 100–102, https://doi.org/10.1016/S0304-8853(00)00077-9.
[7] L. Vandenbossche, S. Jacobs, F. Henrotte, K. Hameyer, Impact of cut edges on magnetization curves and iron losses in e-machines for automotive traction, World Electr. Veh. J. 4 (2011) 587–596, https://doi.org/10.3390/wevj4030587.
[8] A. Schoppa, J. Schneider, C.D. Wuppermann, Influence of the manufacturing process on the magnetic properties of non-oriented electrical steels, J. Magn. Magn. Mater. 215 (2000) 74–78, https://doi.org/10.1016/S0304-8853(00)00070-6.
[9] N. Takahashi, H. Morimoto, Y. Yunoki, D. Miyagi, Effect of shrink fitting and cutting on iron loss of permanent magnet motor, J. Magn. Magn. Mater. 320 (20) (2008) e925–e928, https://doi.org/10.1016/j.jmmm.2008.04.170.
[10] T. Nakata, M. Nakano, K. Kawahara, Effects of stress due to cutting on magnetic characteristics of silicon steel, IEEE Transl. J. Magn. Japan. 7 (6) (1992) 453–457, https://doi.org/10.1109/TJMJ.1992.4565422.
[11] H.A. Weiss, N. Leuning, S. Steentjes, K. Hameyer, T. Andorfer, S. Jenner, W. Volk, Influence of shear cutting parameters on the electromagnetic properties of non-oriented electrical steel sheets, J. Magn. Magn. Mater. 421 (2017) 250–259, https://doi.org/10.1016/j.jmmm.2016.08.002.
[12] A. Peksoz, S. Erdem, N. Derebasi, Mathematical model for cutting effect on magnetic flux distribution near the cut edge of non-oriented electrical steels, Comput. Mater. Sci. 43 (4) (2008) 1066–1068, https://doi.org/10.1016/j.commatsci.2008.02.025.
[13] H.A. Weiss, S. Steentjes, P. Tröber, N. Leuning, T. Neuwirth, M. Schulz, K. Hameyer, R. Golle, W. Volk, Neutron grating interferometry investigation of punching-related local magnetic property deteriorations in electrical steels, J. Magn. Magn. Mater. 474 (2019) 643–653, https://doi.org/10.1016/j.jmmm.2018.10.098.
[14] R. Rygal, A.J. Moses, N. Derebasi, J. Schneider, A. Schoppa, Influence of cutting stress on magnetic field and flux density distribution in non-oriented electrical steels, J. Magn. Magn. Mater. 215 (2000) 687–689, https://doi.org/10.1016/S0304-8853(00)00259-6.
[15] S.V.A. Laakso, A. Väänänen, S. Bossuyt, A. Arkkio, Dull punch line is not a joke – worn cutting edge causes higher iron losses in electrical steel piercing, Robot. Comput. Integr. Manuf. 55 (2019) 141–146, https://doi.org/10.1016/j.rcim.2018.03.006.
[16] H.A. Weiss, P. Trober, R. Golle, S. Steentjes, N. Leuning, S. Elfgen, K. Hameyer, W. Volk, Impact of punching parameter variations on magnetic properties of nongrain-oriented electrical steel, IEEE Trans. Ind. Appl. 54 (6) (2018) 5869–5878, https://doi.org/10.1109/TIA.2018.2853133.
[17] P. Baudouin, M. De Wulf, L. Kestens, Y. Houbaert, The effect of the guillotine clearance on the magnetic properties of electrical steels, J. Magn. Magn. Mater. 256 (1-3) (2003) 32–40, https://doi.org/10.1016/S0304-8853(02)00004-5.
[18] T. Omura, Y. Zaizen, M. Fukumura, K. Senda, H. Toda, Effect of hardness and thickness of nonoriented electrical steel sheets on iron loss deterioration by shearing process, IEEE Trans. Magn. 51 (11) (2015) 1–4, https://doi.org/10.1109/TMAG.2015.2443176.
[19] J. Slota, E. Spišák, L. Kaščák, J. Majerníková, Experimental and finite element analysis of the shear cutting process of electrical steel sheets under various process conditions, in: IOP Conf. Ser. Mater. Sci. Eng., Institute of Physics Publishing, 2019. doi:10.1088/1757-899X/651/1/012084.
[20] L. Vandenbossche, S. Jacobs, D. Van Hoecke, E. Attrazic, Impact of mechanical stresses on the magnetic performance of non-oriented electrical steels and its relation to electric machine efficiency, in: 2015 IEEE Transp. Electrif. Conf. Expo, ITEC 2015. 3 (2015). doi: 10.1109/ITEC.2015.7165801.
[21] E. Gomes, J. Schneider, K. Verbeken, G. Pasquarella, Y. Houbaert, Dimensional effects on magnetic properties of fesi steels due to laser and mechanical cutting, IEEE Trans. Magn. 46 (2010) 213–216, https://doi.org/10.1109/TMAG.2009.2034124.
[22] F. Ossart, E. Hug, O. Hubert, C. Buvat, R. Billardon, Effect of punching on electrical steels: experimental and numerical coupled analysis, in, IEEE Trans. Magn. (2000) 3137–3140, https://doi.org/10.1109/20.908712.
[23] A.J. Moses, N. Derebasi, G. Loisos, A. Schoppa, Aspects of the cut-edge effect stress on the power loss and flux density distribution in electrical steel sheets, J. Magn. Magn. Mater. 215 (2000) 690–692, https://doi.org/10.1016/S0304-8853(00)00260-2.
[24] Y. Kurosaki, H. Mogi, H. Fujii, T. Kubota, M. Shiozaki, Importance of punching and workability in non-oriented electrical steel sheets, J. Magn. Magn. Mater. 320 (20) (2008) 2474–2480, https://doi.org/10.1016/j.jmmm.2008.04.073.
[25] A. Pulnikov, P. Baudouin, J. Melkebeek, Induced stresses due to the mechanical cutting of non-oriented electrical steels, J. Magn. Magn. Mater. 254–255 (2003) 355–357, https://doi.org/10.1016/S0304-8853(02)00853-3.
[26] A. Saleem, D. Goldbaum, N. Brodusch, R. Gauvin, R.R. Chromik, Microstructure and mechanical property connections for a punched non-oriented electrical steel lamination, Mater. Sci. Eng. A. 725 (2018) 456–465, https://doi.org/10.1016/j.msea.2018.04.054.
[27] H. Lee, J.-T. Park, Effect of cut-edge residual stress on magnetic properties in non-oriented electrical steel, IEEE Trans. Magn. 55 (2) (2019) 1–4, https://doi.org/10.1109/TMAG.2018.2866680.
[28] H.M.S. Harstick, M. Ritter, A. Plath, W. Riehemann, EBSD investigations on cutting edges of non-oriented electrical steel, Metallogr. Microstruct. Anal. 3 (4) (2014) 244–251, https://doi.org/10.1007/s13632-014-0148-2.
[29] H. Cao, L. Hao, J. Yi, X. Zhang, Z. Luo, S. Chen, R. Li, The influence of punching process on residual stress and magnetic domain structure of non-oriented silicon steel, J. Magn. Magn. Mater. 406 (2016) 42–47, https://doi.org/10.1016/j.jmmm.2015.12.098.
[30] K. Senda, M. Ishida, Y. Nakasu, M. Yagi, Influence of shearing process on domain structure and magnetic properties of non-oriented electrical steel, J. Magn. Magn. Mater. 304 (2) (2006) e513–e515, https://doi.org/10.1016/j.jmmm.2006.02.139.
[31] G. Loisos, A.J. Moses, Effect of mechanical and Nd:YAG laser cutting on magnetic flux distribution near the cut edge of non-oriented steels, J. Mater. Process. Technol. 161 (1-2) (2005) 151–155, https://doi.org/10.1016/j.jmatprotec.2004.07.061.
[32] K. Bourchas, A. Stening, J. Soulard, A. Broddefalk, M. Lindenmo, M. Dahlen, F. Gyllensten, Quantifying effects of cutting and welding on magnetic properties of electrical steels, IEEE Trans. Ind. Appl. 53 (5) (2017) 4269–4278, https://doi.org/10.1109/TIA.2017.2698400.
[33] N. Alatawneh, A. Saleem, T. Rahman, D.A. Lowther, R. Chromik, Modelling and analysis of the effects of cutting of core laminations in electric machines, IET Electr. Power Appl. 14 (12) (2020) 2355–2361, https://doi.org/10.1049/iet-epa.2020.0218.
[34] T.P. Holopainen, P. Rasilo, A. Arkkio, Identification of magnetic properties for cutting edge of electrical steel sheets, IEEE Trans. Ind. Appl. 53 (2) (2017) 1049–1053, https://doi.org/10.1109/TIA.2016.2638405.
[35] M. Bali, H. De Gersem, A. Muetze, Determination of original nondegraded and fully degraded magnetic characteristics of material subjected to laser cutting, IEEE Trans. Ind. Appl. 53 (5) (2017) 4242–4251, https://doi.org/10.1109/TIA.2017.2696479.
[36] L. Vandenbossche, S. Jacobs, X. Jannot, M. McClelland, J. Saint-Michel, E. Attrazic, Iron loss modelling which includes the impact of punching, applied to high-efficiency induction machines, in: 2013 3rd Int. Electr. Drives Prod. Conf. EDPC 2013 – Proc., 2013. doi: 10.1109/EDPC.2013.6689720.

[37] Z. Gmyrek, A. Cavagnino, Analytical method for determining the damaged area width in magnetic materials due to punching process, in: IECON Proc. (Industrial Electron. Conf., 2011). doi:10.1109/IECON.2011.6119573.
[38] C.-C. Chiang, M.-F. Hsieh, Y.-H. Li, M.-C. Tsai, Impact of electrical steel punching process on the performance of switched reluctance motors, IEEE Trans. Magn. 51 (11) (2015) 1–4, https://doi.org/10.1109/TMAG.2015.2449661.
[39] X. Xiao, F. Muller, G. Bavendiek, N. Leuning, P. Zhang, J. Zou, K. Hameyer, Modeling of Scalar Dependencies of Soft Magnetic Material Magnetization for Electrical Machine Finite-Element Simulation, IEEE Trans. Magn. 56 (2) (2020) 1–4, https://doi.org/10.1109/TMAG.2019.2950527.
[40] R. Sundaria, A. Lehikoinen, A. Hannukainen, A. Arkkio, Higher-order finite element modeling of material degradation due to cutting, in: 2017 IEEE Int. Electr. Mach. Drives Conf. IEMDC 2017, 2017. Doi: 10.1109/IEMDC.2017.8002278.
[41] R. Sundaria, A. Lehikoinen, A. Hannukainen, A. Arkkio, A. Belahcen, Mixed-order finite-element modeling of magnetic material degradation due to cutting, IEEE Trans. Magn. 54 (6) (2018) 1–8, https://doi.org/10.1109/TMAG.2018.2811385.
[42] S. Elfgen, S. Steentjes, S. Bohmer, D. Franck, K. Hameyer, Continuous local material model for cut edge effects in soft magnetic materials, IEEE Trans. Magn. 52 (5) (2016) 1–4, https://doi.org/10.1109/TMAG.2015.2511451.
[43] F. Martin, U. Aydin, R. Sundaria, P. Rasilo, A. Belahcen, A. Arkkio, Effect of punching the electrical sheets on optimal design of a permanent magnet synchronous motor, IEEE Trans. Magn. 54 (3) (2018) 1–4, https://doi.org/10.1109/TMAG.2017.2768399.
[44] P. Sudharshan Phani, W.C. Oliver, A critical assessment of the effect of indentation spacing on the measurement of hardness and modulus using instrumented indentation testing, Mater. Des. 164 (2019) 107563, https://doi.org/10.1016/j.matdes.2018.107563.
[45] A. International, Standard test methods for tension testing of metallic materials, 2016.
[46] M. Kamaya, Assessment of local deformation using EBSD: quantification of accuracy of measurement and definition of local gradient, Ultramicroscopy 111 (8) (2011) 1189–1199, https://doi.org/10.1016/j.ultramic.2011.02.004.
[47] M. Kamaya, Measurement of local plastic strain distribution of stainless steel by electron backscatter diffraction, Mater. Charact. 60 (2) (2009) 125–132, https://doi.org/10.1016/j.matchar.2008.07.010.
[48] M. Kamaya, A.J. Wilkinson, J.M. Titchmarsh, Quantification of plastic strain of stainless steel and nickel alloy by electron backscatter diffraction, Acta Mater. 54 (2) (2006) 539–548, https://doi.org/10.1016/j.actamat.2005.08.046.
[49] M. Kamaya, A.J. Wilkinson, J.M. Titchmarsh, Measurement of plastic strain of polycrystalline material by electron backscatter diffraction, Nucl. Eng. Des. 235 (6) (2005) 713–725, https://doi.org/10.1016/j.nucengdes.2004.11.006.
[50] L.N. Brewer, M.A. Othon, L.M. Young, T.M. Angeliu, Misorientation mapping for visualization of plastic deformation via electron back-scattered diffraction, Microsc. Microanal. 12 (01) (2006) 85–91, https://doi.org/10.1017/S1431927606060120.
[51] H.M.S. Harstick, M. Ritter, W. Riehemann, Influence of punching and tool wear on the magnetic properties of nonoriented electrical steel, IEEE Trans. Magn. 50 (4) (2014) 1–4, https://doi.org/10.1109/TMAG.2013.2285243.
[52] W. Wu, H. Cao, H. Ou, Z. Chen, X. Zhang, Z. Luo, S. Chen, R. Li, Effects of punching process on crystal orientations, magnetic and mechanical properties in non-oriented silicon steel, J. Magn. Magn. Mater. 444 (2017) 211–217, https://doi.org/10.1016/j.jmmm.2017.07.003.
[53] S.J. Bull, On the origins and mechanisms of the indentation size effect, Zeitschrift Für Met. 94 (7) (2003) 787–792, https://doi.org/10.3139/146.030787.
[54] J.M. Makar, B.K. Tanner, The in situ measurement of the effect of plastic deformation on the magnetic properties of steel, J. Magn. Magn. Mater. 184 (2) (1998) 193–208.
[55] F.J.G. Landgraf, M. Emura, K. Ito, P.S.G. Carvalho, Effect of plastic deformation on the magnetic properties of non-oriented electrical steels, J. Magn. Magn. Mater. 215 (2000) 94–96, https://doi.org/10.1016/S0304-8853(00)00075-5.
[56] D. Singh, K. Mökkönen, J. Poutala, P. Rasilo, A. Belahcen, R. Kouhia, Preliminary results on the effect of plastic deformation on magnetic properties, Raken. Mek. 50 (2017) 372–375, https://doi.org/10.23998/rm.65180.
[57] V.E. Iordache, F. Ossart, E. Hug, Magnetic characterisation of elastically and plastically tensile strained non-oriented Fe-3.2%Si steel, J. Magn. Magn. Mater. 254-255 (2003) 57–59, https://doi.org/10.1016/S0304-8853(02)00748-5.
[58] N. Leuning, S. Steentjes, M. Schulte, W. Bleck, K. Hameyer, Effect of elastic and plastic tensile mechanical loading on the magnetic properties of NGO electrical steel, J. Magn. Magn. Mater. 417 (2016) 42–48, https://doi.org/10.1016/j.jmmm.2016.05.049.
[59] D.L. Rodrigues-Jr, J.R.F. Silveira, G.J.L. Gerhardt, F.P. Missell, F.J.G. Landgraf, R. Machado, M.F. de Campos, Effect of plastic deformation on the excess loss of electrical steel, IEEE Trans. Magn. 48 (4) (2012) 1425–1428, https://doi.org/10.1109/TMAG.2011.2174214.
[60] N. Leuning, S. Steentjes, H.A. Weiss, W. Volk, K. Hameyer, Magnetic material deterioration of non-oriented electrical steels as a result of plastic deformation considering residual stress distribution, IEEE Trans. Magn. 54 (11) (2018) 1–5, https://doi.org/10.1109/TMAG.2018.2848365.
[61] H. Naumoski, B. Riedmüller, A. Minkow, U. Herr, Investigation of the influence of different cutting procedures on the global and local magnetic properties of non-oriented electrical steel, J. Magn. Magn. Mater. 392 (2015) 126–133, https://doi.org/10.1016/j.jmmm.2015.05.031.
[62] J. Reinert, A. Brockmeyer, R.W.A.A. De Doncker, Calculation of losses in ferro- and ferrimagnetic materials based on the modified Steinmetz equation, IEEE Trans. Ind. Appl. 37 (4) (2001) 1055–1061, https://doi.org/10.1109/28.936396.